Journal of the Brazilian Society of Mechanical Sciences and Engineering (2023) 45:164
https://doi.org/10.1007/s40430-023-04077-1

REVIEW

A critical review of wire arc additive manufacturing of nickel-based alloys: principles, process parameters, microstructure, mechanical properties, heat treatment effects, and defects

Manickam Bhuvanesh Kumar[1,2] · **Paulraj Sathiya**[1] · **Sathyamangalam Munusamy Senthil**[2]

Received: 27 June 2022 / Accepted: 30 January 2023 / Published online: 22 February 2023

Abstract
Wire arc additive manufacturing (WAAM) is capable of fabricating medium-to-large-scale parts due to its higher deposition rates. The mechanical and metallurgical characteristics of WAAMed parts are better compared to other additive manufacturing techniques. Since the technology has grown, a wide range of metals are processed by WAAM in recent days. Nickel (Ni)-based superalloys are superior in terms of oxidation resistance, high-temperature mechanical performance, and microstructural characteristics. The selection of WAAM techniques, input parameters, resulting microstructure, post-processing treatments, and the defects can influence the final mechanical properties. The WAAMed Ni-based superalloys show inhomogeneous microstructure and mechanical properties from bottom to top layers. To obtain the homogeneous and improved mechanical properties, still there is a strong need to understand the underlying physical metallurgical mechanisms. In this context, this paper reports a present-day review on the process parameters, microstructural characteristics, mechanical properties, corrosion behaviour, and defects of WAAMed Ni-based superalloys. Adapting the strategies like interpass cooling, post-deposition heat treatment, and solution annealing improves the mechanical properties and can help to obtain homogeneous characteristics. More penetrative research works should be carried out to analyse fatigue and corrosion properties of WAAMed Ni-based superalloys for future industrial applications. Additionally, process parameters optimization and better control over quality are the other aspects to be focused by further studies.

Keywords Wire arc additive manufacturing (WAAM) · Ni-based alloys · Microstructure · Heat treatment · Corrosion · Defects

1 Introduction

1.1 Overview of wire arc additive manufacturing of alloys

Additive manufacturing (AM) techniques can effectively manufacture most superalloys used in aeronautics, aerospace, marine, and automotive sectors by reducing their manufacturing cost compared to conventional manufacturing [1]. The AM can minimize the material requirements and fabrication time [2, 3]. AM processes enable better flexibility to convert the feedstock material into a required part, thus provide a better buy-to-fly (BTF) ratio. Since AM techniques are reliable and innovative to fabricate three-dimensional (3D) parts directly from computer-aided design (CAD) models, the researchers now focus more on developing metal additive manufacturing (MAM) techniques. The MAM techniques can manufacture large-scale engineering components inexpensively if the deposition rates are increased along with its capability of fabricating complex structures [4]. Many MAM techniques have been developed to deposit metallic materials with higher precision and dimensional accuracy under the categories of direct energy deposition (DED), powder bed fusion (PBF), powder jetting, and sheet lamination as per the American society for testing and materials

Technical Editor: Izabel Fernanda Machado.

✉ Manickam Bhuvanesh Kumar
bhuvanesh85@gmail.com

1 Department of Production Engineering, National Institute of Technology Tiruchirappalli, Tiruchirappalli, Tamil Nadu, India

2 Present Address: Department of Mechanical Engineering, Kongu Engineering College, Perundurai, Tamil Nadu, India

(ASTM) International Committee F42 [5]. Comparing to the other MAM techniques, wire arc additive manufacturing (WAAM) can deposit metals at higher deposition/fabrication rates using a wire form feed stock material. The WAAM process belongs to the DED category which is also known in two different names as structural weld build up (American) and shape welding (European) [6, 7]. Over a period, WAAM has been given several names like 3D welding, solid freeform fabrication (SFF), shape melting (SM), and shape metal deposition (SMD) [8]. The WAAM has been exercised since 1920 but becoming popular in the recent years [9]. The WAAM has been effectively used starting from the manufacturing of nuclear components in German during late twentieth century to the present-day applications like aerospace (wings ribs, stiffened panels), architecture, and marine [7, 10].

The WAAM uses an electric arc as a heat source to melt and deposit the metallic wire, similar to the conventional welding process. The wire form of feedstock material is inexpensive than the powder form used by other laser-based AM techniques which makes it economical compared to other DED techniques. The wire form of filler wire costs only about 10% of the same weight of powder metal [11]. Modern automation technologies in welding advances the WAAM process to be cost-effective, eco-friendly, structurally flexible and capable of processing a wide range of metallic materials such as aluminium (Al)-based [12, 13], steel-based [14, 15], titanium (Ti)-based [16, 17], magnesium (Mg)-based [18, 19], nickel (Ni)-based [20, 21] alloys, and many more. Superalloys are the category of materials that can retain some of their room temperature mechanical and physical properties even at higher working temperatures [22]. This is an essential characteristic for aerospace components. Having several advantages, Ni-based alloys being the base for superalloys holds a melting temperature of 1453 °C and high hardness makes it difficult to get manufactured by conventional manufacturing processes such as casting and machining. The WAAM can produce fully dense components of these alloys efficiently with less cost and wastage compared to other AM techniques [23]. Recently, there are many experimental studies that reported the microstructure, mechanical properties, distortion, residual stresses, defects, corrosion resistance, and process parameters of WAAMed Ni-based alloys [21, 23–25]. Compared to the wrought metal, the mechanical and microstructural characteristics of WAAMed Ni-based alloys are quite different and show anisotropy behaviour [21, 24]. The selection of WAAM techniques, optimizing the process parameters, minimizing the heat input, post-deposition heat treatments, inter-pass cooling strategies (ICS), solution annealing, etc., can help to achieve better microstructural, and mechanical characteristics.

1.2 Need and aim of this review

There have been a number of review articles reported in the literature on investigating the microstructure, mechanical properties, post-processing heat treatment effects, and corrosion properties of additively manufactured metallic materials using different AM techniques [6, 26–29]. These techniques include laser-based AM [30, 31], electron beam-based AM [32], inkjet-based AM [33], ultrasonic AM [34], and WAAM [35, 36] among the others. But the comprehensive review articles for WAAMed superalloys were found to be very few in the literature. Two most inclusive reviews on WAAMed Ni-based alloys available in the literature are by Wu et al. [37] and Dhinakaran et al. [38]. Wu et al. [37] provided an overview about WAAM, metals used in WAAM, common defects arise in WAAMed components, and the methods to improve the component's quality. These authors have comprehensively summarized the metallurgical characteristics and mechanical properties of WAAMed metals including superalloys such as Ti-based alloys and Ni-based alloys. Dhinakaran et al. [38] reviewed the WAAM of Ni-based alloys. These authors have provided an overview of different welding techniques adapted for WAAM process and presented the suitability of different Ni-based alloys for WAAM process. Further, the measures to overcome the shortcomings, the effect of residual stresses and porosity were briefed. But none of these reviews provided a detailed investigation on the characterization of WAAMed Ni-based alloys and the present review focus on this aspect.

This review is mainly centred on presenting parameter setting, microstructure, mechanical, and corrosion properties of WAAMed Ni-based alloys with the available relevant data from the literature. The quality of WAAMed Ni-based alloys in terms of microstructure, mechanical properties and corrosion properties has been improved by adapting post-processing techniques in the recent past but there is a lack of summary on how these appreciable properties were obtained. Also, there are no articles summarizing the defects in WAAMed Ni-based alloys. The present review aims to fill this gap by comprehensively summarizing the detailed characterization of different grades of Ni-based alloys manufactured by different WAAM techniques from the literature. We also intend to discuss the positive effects of post-processing heat treatment to eliminate the defects.

Even though these research works reported the successfulness of WAAM of Ni-based alloys, still there is no holistic view to understand the underlying physical metallurgical mechanisms, and this review is the first of its kind. In light of this, a present-day review on the WAAM of different grades of Ni-based alloys such as Inconel 625, Inconel 718, ATI 718PLUS, nickel–titanium alloy, and other Ni-based alloys in terms of their process parameters, microstructure, mechanical properties, heat treatment effects, corrosion behaviour, and defects are presented in this paper. To explore the future research opportunities, the challenges, limitations, and future research directions of WAAM of Ni-based alloys are presented at the end.

2 Wire arc additive manufacturing

WAAM uses a feedstock material in wire form combined with an arc welding-based deposition technique which makes it a higher deposition AM process. There are other wire-based AM processes like electron beam freeform fabrication (EBFF) that offer high deposition efficiency and concentrated energy density [39]. Owing to the requirements such as vacuum environment, more complicated setup of EBFF, WAAM is becoming an emerging technique around the global research community. The common welding techniques adapted in WAAM are gas tungsten arc welding (GTAW), gas metal arc welding (GMAW), cold metal transfer (CMT), and plasma arc welding (PAW). The GTAW produces clean and high-quality depositions [40, 41]. The GMAW due to its higher heat input and large melt pool has a limitation to produce thin-walled structures with smooth outside surfaces [42, 43]. To overcome this issue, a significant technique called CMT is widely adapted in which electrode is moved forth and back at given frequencies to reduce the arcing time. Discontinuous nature of arc leads to smooth droplet-based deposition of metal, and minimized heat supply [44–46]. Research works also acclaim the modification of these processes, namely super-GTAW, hot wire GTAW (HWGTAW), tandem–GMAW, variable polarity CMT, pulsed CMT (PCMT) and pulsed PAW (PPAW) [47, 48]. However, the process setting and production rate of intended component is directly depending on the selection of WAAM technique. The comparison of different WAAM techniques based on the source of energy, electrode type, deposition rates and the specific features with is presented in Table 1.

2.1 A robotic system for WAAM

The WAAM setups mainly use an automated industrial robot to provide an articulated multi-axis motion of welding torch on the desired path. In general, two different designs of the WAAM systems are available. The systems are basically designed to shield the supplied inert gases from the environment. One system uses a completely closed chamber similar to PBF, and another system uses an available existing shielding mechanisms. To produce large sized parts, the robots are positioned on the linear rails to increase the working space. Such setups can fabricate large components of several metres in length. A setup used for WAAM and process monitoring in all aspects is shown in Fig. 1.

Table 1 Comparison of different techniques used in WAAM

Technique	Source of energy	Electrode type	Deposition rate (kg/hr)	Features	References
GMAW-based WAAM	GMAW	Consumable wire	3–4	Produces spatter Arc stability is poor	[49]
	CMT	Consumable wire with reciprocating feed	2–3	Zero spatter Low heat input Significant process tolerance	[50]
	PCMT	Reciprocating consumable wire with pulsed arc	2–3	Zero spatter Low heat input	[51]
	Variable polarity CMT	Consumable wire with reciprocating feed	3–5	Cooler than CMT Dissimilar metals addition	[51, 52]
	Tandem–GMAW	Two consumable wires	6–8	Enables the fabrication of intermetallic materials	[53]
GTAW-based WAAM	GTAW	Non-consumable	1–2	Separate wire feed Need of torch and wire rotation	[54]
	Super-GTAW	Non-consumable	6–7	Uses C-Filler Higher energy efficiency	[55, 56]
	HWGTAW	Non-consumable	8	Constant bead geometry Stable and spatter-free process	[48]
PAW-based WAAM	Plasma	Non-consumable	2–4	Separate wire feed	[54]
	Pulsed plasma	Non-consumable	2–4	High manufacturing efficiency Variable polarity current is needed	[57]

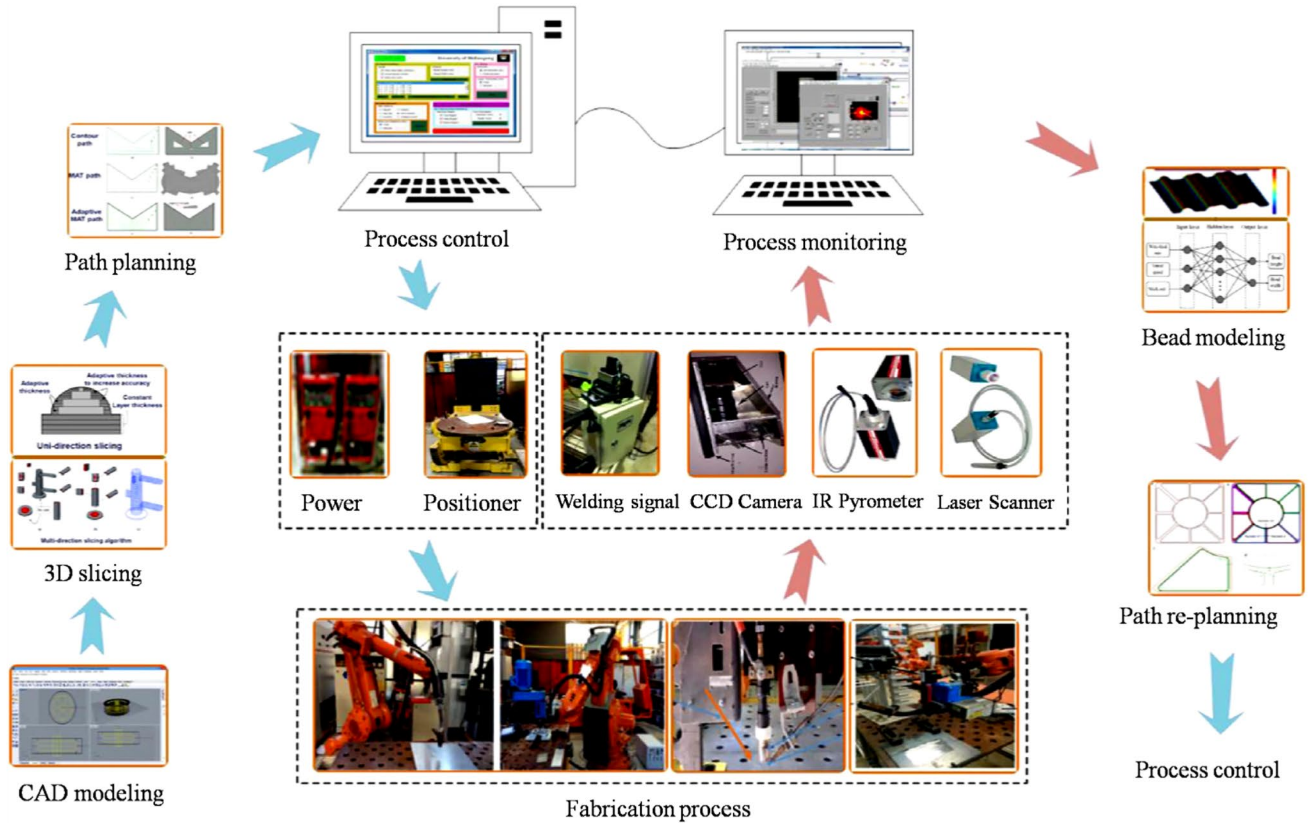

Fig. 1 A typical WAAM setup used in the University of Wollongong (Courtesy of Wu et al. [37])

The WAAM process starts with designing a required 3D model using CAD software, slicing and path planning for the designed model, deposition using an automated robotic system, and ends by post-processing [58]. The deposition parameters and robotic motion required for producing defect-free quality metal addition are generated by the slicing and process planning softwares [59–61]. Additionally, the process-dependent defects can be eliminated by optimizing the process parameters [62]. The precise movement of welding torch attached to robot arm through a planned path deposits the material on a metal substrate as a layer. Repeating this action offers a layer by layer deposition of metal to build a 3D component.

Upon the solidification of molten metal layer over a cold substrate, the subsequent thermal contraction of metal layer generates tensile and compressive stresses respectively on the deposited layer and substrate. These locked-in stress levels can be elevated to a remarkable level while depositing numerous metal layers during the building process. However, the metal undergoes a number of heating and cooling cycles alternatively that trigger stress accumulation and relaxation. After deposition, the tensile and compressive stresses can be observed respectively on the built wall and substrate and are higher than the yield strength that causes bending distortion leading to a warpage [63]. According to the earlier studies, the deposition strategies and the size of melt pool are the influencing factors for the distribution and magnitude of the developed stresses [64]. Hence, it important to take into account the residual stresses on the selection of deposition strategy and perform design of parts during WAAM process.

Recent advanced WAAM systems are equipped with feedback sensors to measure, in-process monitoring, and control the welding signals [22], geometry of deposition [65], behaviour of metal transfer [10], and interpass cooling [66] to obtain high product quality and efficient process [67–69]. These advancements enable WAAM to process most of the metallic materials with feature-based structures as shown in Fig. 2. But still WAAMed components show surface irregularities and needs a further machining process as shown in Fig. 3. Despite of these challenges, MAM using WAAM became the present and future thrust area for research.

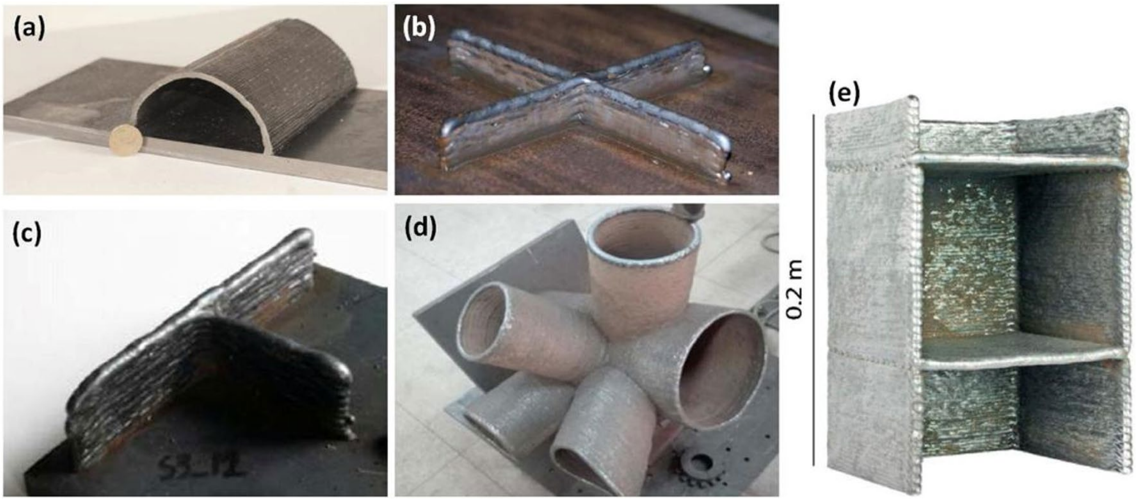

Fig. 2 Different feature-based build structures produced by WAAM **a** enclosed **b** cross-intersections **c** T-intersections **d** pipe joints and **e** features in horizontal plane without support (Courtesy of Michel et al. [70], and [4])

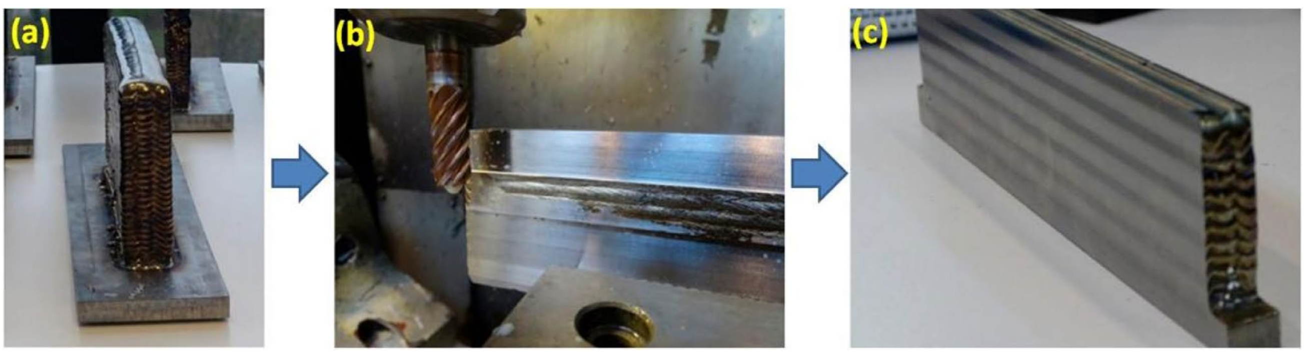

Fig. 3 WAAM-deposited Ti wall **a** as-deposited **b** secondary machining operation milling and **c** machined wall (Courtesy of Alonso et al. [17])

3 Wire arc additive manufacturing of Ni-based alloys

Superalloys are high-performance alloy materials that can serve their functions and handle heavy loads even at high temperature and corrosive environments. For that reason, Ni-based superalloys take part majorly (around 50% by weight) in aircraft engines, particularly in the turbine and combustor segments. Ni-based superalloys can retain their mechanical properties even at elevated temperature and load conditions [71]. Researchers around the globe have been investigating the additively manufactured Ni-based superalloys for their applicability in aerospace and petroleum industries due to their high-temperature stability. The mechanical properties such as tensile and yield stresses of WAAM fabricated Ni-based superalloys generally meets the standards of ASTM [72]. Different grades of Ni-based superalloy depositions using WAAM have been characterized for their microstructure formation, mechanical properties, defects, and other characteristics by previous researchers. The following sections provide a brief about previous research works reported on different Ni-based alloys fabricated using WAAM.

3.1 Inconel 625

Inconel 625 is a Ni-based superalloy with good weldability and high resistance to hot corrosion and fatigue properties. Its superior strength is derived mainly by molybdenum and niobium in a Ni–Cr matrix due to solid solution hardening [73]. Since heat source is the primary factor that decides upon the quality of formed parts, different WAAM techniques and strategies have been carried out on Inconel 625. Xu et al. [74] examined the microstructure, and mechanical properties of PPAW-based WAAM fabricated Inconel625alloy. The strategies such as continuous deposition strategy (CDS) and ICS have been adapted during the fabrication process. CDS produced no appreciable effects, but ICS improved the mechanical properties and surface quality. Jiang et al. [75] investigated the influence of two different torch trajectories on the thermal input, grain growth, and mechanical properties of CMT-WAAM fabricated Inconel 625 alloy. The two-pass multi-layer trajectory exhibits improved properties compared to the oscillation pass trajectory. Similarly, Cheepu et al. [56] studied the effect of single-pass oscillation and multi-pass layering strategies using the super-TIG-WAAM process. Multi-pass layering strategies with zig-zag and stringer layering depositions have resulted in a refined grain structure.

3.2 Inconel 718 & ATI 718PLUS

Different industries use Inconel 718 alloy due to its stability at higher temperature levels. At various working conditions, Inconel 718 exhibits high fatigue life with lower levels of residual stresses. Though the yield strength is slightly less than its residual stress, it is influenced by warping, delamination, and buckling [38]. But the properties and applicability of WAAM-deposited Inconel 718 alloy were investigated by several research works in the recent past. Kindermann et al. [76] investigated the process parameters and heat treatment effects on the CMT-based WAAM built Inconel 718 alloy. Melt pool imaging and electrical transient analysis were done to examine the process stability. Optimized parameters resulted in improved output responses in terms of mechanical and microstructural characteristics. Similarly, Xu et al. [77] investigated the mechanical properties of CMT-based MIG-WAAM fabricated Inconel 718. Additionally, the effects of oxide formation and heat treatment have been studied experimentally. It was argued that heat treatment has no further improvement on the mechanical properties of WAAM fabricated Inconel 718. But the ageing effect can show different values in mechanical properties such as hardness [78]. Wang et al. [79] fabricated a thin wall using PAAM. It was found that reduction in heat input for every successive layer minimized its accumulation and resulted in diverse grain morphologies. Also, the mechanical properties were remarkably enhanced compared with as-cast Inconel 718.

Allegheny Technologies Incorporated (ATI), a speciality metal manufacturer, has developed an advanced version of Inconel 718 called ATI 718PLUS by making few modifications on the chemical composition which resulted in good manufacturability and increased properties compared to Inconel 718 and Waspaloy. Table 2 shows the comparison of chemical composition between Inconel 718 and ATI 718PLUS [38]. Retaining the advantageous properties of Inconel 718, ATI 718PLUS additionally offers improved thermal stability than Inconel 718 and used in power plants and aero-engines. The manufacturability of ATI 718PLUS using WAAM and its process effects have been investigated recently by few research studies. Asala et al. [80] performed a detailed microstructural analysis of TIG-WAAM fabricated ATI 718PLUS superalloy. It was observed that WAAM produced microstructure was not in favour of improving mechanical properties. Hence, it required the development of innovative heat treatment methods. Later, Oguntuase et al. [81] examined the influence of post-fabrication heat treatments on the WAAM built ATI 718PLUS superalloy. The post-deposition heat treatments reduced the anisotropic effects of η phase present in the microstructure, which improved the mechanical properties. The studies related to strain-deformation behaviour [82] and hot corrosion behaviour [83] on the same material helps to improve the process and microstructural characteristics further.

3.3 Nickel–titanium alloy

Nickel–titanium (Ni–Ti) alloy is a special category of Ni-based alloy due to its shape memory capability. Ni–Ti is used in various fields such as aerospace, robotic, and automotive due to its superelastic property. The reversible martensitic transformation of crystals attributes to these special properties [84]. Good damping, low stiffness, and corrosion resistance are the other characteristics of Ni–Ti alloy [85]. Ni–Ti alloy has significantly less impurities and bone alike elastic modulus; hence, it is used in medical field also. The manufacturability of this alloy has been experimented by several powder bed-based AM techniques such as selective laser sintering (SLS), selective laser melting (SLM), and electron beam melting (EBM) [86]. But porosity and lack of fusion are the common defects reported by those powder bed fusion techniques.

Recently, WAAM acquired significant attention in fabricating Ni–Ti alloy due to its higher and melt-based deposition similar to SLM. Initial fabrication results of Ni–Ti alloy through WAAM showed increased tensile strength and hardness, but ductility showed a negative trend [87]. Retaining its superelastic behaviour under tensile load conditions by fusion-based AM is challenging. The experimental results produced by Zeng et al. [88] have proven the potential of

Table 2 Comparison of chemical compositions between Inconel 718 and ATI 718PLUS

Element	Cr	Fe	Nb	Mo	Ti	Al	C	P	B	Co	W	Ni
Inconel 718	18.1	18	5.4	2.9	1	0.45	0.025	0.007	0.004	0	0	Bal
ATI 718PLUS	18	10	5.45	2.8	0.7	1.45	0.02	0.007	0.004	9	1	Bal

WAAM to fabricate Ni–Ti-like functional materials. It was reported that TIG-WAAM fabricated Ni–Ti alloy exhibited superelastic performance under tensile load circumstances. Wang et al. [89] characterized the microstructure and mechanical properties of Ni–Ti coatings on Ti6Al4V alloy made through the WAAM process. The dense and crack-free coatings exhibited excellent wear resistance, microhardness, and microstructural characteristics. It is evident that WAAM can be used to produce coatings of functional materials to obtain improved functional characteristics of surfaces. Shen et al. [90] studied the thermal phase evolution of Ni53Ti47 binary alloy fabricated through WAAM. As-deposited alloy showed the presence of micro-strain, which was induced by residual stresses during heating. The study opened a scope for further research directions on the post-fabrication heat treatments.

There are also advancements in the existing WAAM process to improve the phase transformation characteristics, melt pool instability, distortion and residual stresses of Ni–Ti alloy. Wang et al. [91] deposited dual wires using WAAM to investigate the phase transformation, crystallographic arrangement, and mechanical properties of Ni–Ti alloy. Different deposition currents revealed different results and were helpful to optimize the parameters of WAAM-based Ni–Ti deposition. Singh et al. [92] have used laser marking-supported WAAM process to investigate the mechanical properties and surface morphology of Ni–Ti thin walls. With the help of laser marking, WAAM was successfully able to produce thin walls with reduced track widths. Also, the reduction in surface energy appreciably reduced the surface roughness, distortion, and other defects. This can be significantly making contributions to the fabrication of thin and complex geometries using WAAM.

3.4 Other Ni-based alloys

Other superalloys of interest from the Ni-based cluster are Inconel 825, hastelloy, nickel–copper (Ni–Cu), waspaloy, RENE-41, and nimonic. Very few articles have been found to discuss the application of WAAM to fabricate these alloys. Bharat Kumar and Anandakrishnan [93] investigated the influence of process parameters on the layer geometry of MIG-WAAM-deposited Inconel 825. The process parameters such as the velocity of welding, wire feed speed (WFS), and input voltage have been analysed to obtain an optimal layer width but no further detailing on the microstructure evolution has been reported. Hastelloy is a Ni-based alloy with higher resistance to acidic reactions along with superior mechanical properties. Therefore, hastelloy has been used in extremely corrosive environments. The feasibility of WAAM to fabricate hastelloy components has been demonstrated by Dinovitzer et al. [94]. The effect of WAAM process parameters such as WFS, travel speed (TS), input current, and argon flow rate on the bead geometry and microstructure have been investigated. Complete fusion between the interface layers with no oxide formation helped to analyse the grain formation and distribution. In another study, Qiu et al. [95] fabricated a thin wall of hastelloy-C276 using GTAW-WAAM process. Though no visible defects were noticed, anisotropy in mechanical properties was found. But microhardness has been evenly distributed throughout the samples. The materials need to be integrated using advanced technologies for applications that require different properties at different locations. WAAM is capable of bonding different functional materials successfully without compromising their inherent properties. To check this feasibility on hastelloy, Rajesh Kannan et al. [96] bonded SS904L with hastelloy using WAAM process and found excellent bonding characteristics. The tensile strength of the samples exhibited higher values than wrought materials.

Ni–Cu from Ni-based alloys family is also called monel alloy first discovered in International Nickel Company INCO by Robert Crooks Stanley in 1901. Monel alloys are costlier compared with other metals for corrosive and thermal applications. Generally, these alloys are fabricated by metal forming processes, but WAAM is an alternative manufacturing process to manufacture its complex parts due to inexpensive manufacturing setup. Marenych [97] investigated the microstructure and mechanical properties of CMT-WAAM fabricated Monel K500 and FM60 alloys. From this study, it is evident that WAAM can replace the conventional manufacturing processes effectively for handling costly materials like Ni–Cu alloys. The results exhibited excellent microstructural and mechanical characteristics compared to traditional manufacturing. The heat treatment process with appropriate temperatures on WAAM fabricated Ni–Cu alloys can initiate the precipitation strengthening process, resulting in enhanced mechanical properties [98]. Waspaloy surpasses the Inconel 718 alloy with its increased creep strength and increased percentage of Cr (19.5%) and Co (13.5%) without Fe content [99]. But no significant research works have been found for other Ni-based alloys such as waspaloy, nimonic, and RENE-41 by WAAM Process.

4 Characterization of WAAMed Ni-based superalloys

4.1 Process parameters and their levels

Process parameters are the major driving factors for the product quality and performance of any manufacturing process. Although the surface finish is one of the measures of product and process quality [100, 101], the surface finish of as-deposited WAAM components is poor. More importantly, the quality is assessed based on the evolution of microstructures, mechanical properties, physical properties, geometrical requirements, and other functional characteristics such as resistance to corrosion, wear, acidic reactions, etc. [102]. These characteristics highly rely on the process parameters of WAAM, which can be controlled within specific levels without compromising the deposition rates. Different WAAM process parameters and their levels used for successful deposition of Ni-based alloys from the recent studies are shown in Table 3. The WFS, input current, and voltage were major influencing factors for the complete deposition of wire metal without visible defects. The selection of appropriate combination of these parameters can also help in deciding the width and height of the deposition.

Majority of the researchers have used pure argon [76–79], and few have used Ar 93% + H_2 7% [56], and Ar 70% + He 30% [105] as shielding gases. Besides the stated process parameters from Table 3, the researchers have used different torch-to-substrate distances (TSD) for various metals. For Ni-based alloys, TSD values were generally varied from 10 to 20 mm, and electrode to work piece distance was maintained around 3.5 mm [78, 91, 93]. The TSD values were adjusted through trial runs to get better arc stability and

Table 3 Major WAAM process parameters and their levels used to fabricate Ni-based alloys

Feed wire	WAAM type (Ref.)	Wire feed speed (WFS) (m/min)	Power supply (voltage & current)	Travel speed (TS) (mm/min)	Torch angle (deg)	Flow rate (L/min) of shielding gas	Interpass cooling time/temperature	Wire dia (mm), Layer thickness (mm), Overlap rate (%)
Inconel 625	Super-TIG [56]	1.25	I: 285	200	90°	25 (Ar 93% + H_2 7%)	80 °C	1.2, 2–3, –
	MIG [103]	1	V: 26 I: 250	540	–	15 (100% Ar)	300 °C	1.2, 1.34, –
	PAW [74]	1.50	I: 230	230	–	15 (100% Ar)	300 s	1.2, 1.4, 40%
	CMT [104]	6.50	V: 12.5 I: 130	800	90°	15 (100% Ar)	120 s	1.2, 6–7, –
	CMT [105]	6.50	V: 14.6 I: 148	480–600	90°	15 (Ar 70% + He 30%)	400 °C	1.2, 3.5, 55%
Inconel 718	CMT-MIG [77]	7.00	–	360	90°	15	180 s	1.2, 2.8, –
	CMT [76]	6–10	–	200–800	90°	15 (100% Ar)	80 °C	1.2, 3, –
	CMT [78]	4.80	V: 13.4 I: 120	500	90°	20 (100% Ar)	0–60 s	1.2, 10, –
	PPAW [79]	2	V: 14.3–19.6 I: 120–300	150	–	100% Ar	15 s	1.2, 1.37, –
	TIG [106]	0.5	I: 100	130	–	100% Ar	–	0.787, –, –
ATI 718PLUS	TIG [83]	0.4	I: 100	100	–	15 (100% Ar)	–	1.6, 4, –
	TIG [81]	0.4	I: 100	100	–	15 (100% Ar)	–	0.8, 5.5, 75%
Ni–Ti	GTAW [91]	Ni: 0.51 Ti: 0.7	I: 80, 100, 120	95	30° & 60°	15 (100% Ar)	90 s	1, –, –
	TIG [88]	0.9	I: 75	300	90°	15 (100% Ar)	60 s	0.7, 1, –
	GTAW [90]	Ni: 0.56 Ti: 0.80	I: 140	95	90°	–	400 °C	0.9, 0.94, –
	GTAW [89]	Ni: 0.41 Ti: 0.24	I: 50, 60, 70	95	30° & 60°	15 (100% Ar)	90 s	1.2 & 0.9, 1.91, –
Hastelloy	TIG [94]	0.2–0.29	I: 50–59	84–120	90°	20–35 (100% Ar)	0	1.2, 1, –
	GTAW [95]	1	V: 13 I: 140	100	30°	15 (100% Ar)	60 s	1.2, 0.9, –
	GMAW[96]	–	V: 16.4 I: 160	250	–	100% Ar	–	1.2, 3.4, 55%
Monel K500	CMT [107]	8.3	V: 19.1 I: 157	400	90°	100% Ar	–	1.2, 2.2, –
FM60			V: 15.4 I: 146					

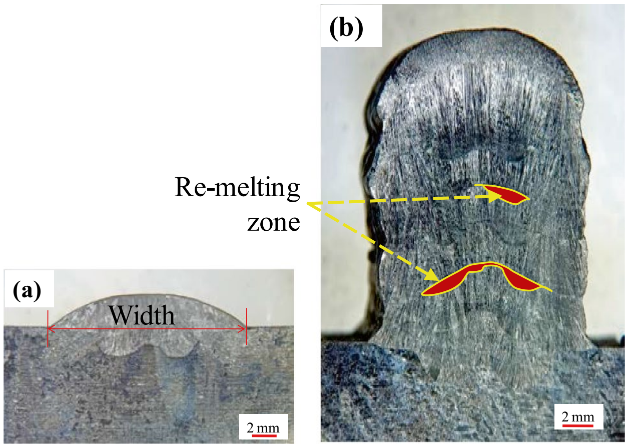

Fig. 4 **a** Maximum width obtained in the deposition of Inconel 825 at 3 m/min TS, 7 m/min WFS and, 21 V **b** Successful deposition of defect-free Inconel 825 wall using CMT-MIG welding process (Courtesy of Bhuvanesh Kumar et al. [108])

smooth deposition throughout the deposition of entire layer. Recent intelligent power systems can adjust the other parameters based on the major input parameters fed. The parameter levels are decided based on the deposition rate and the physical requirements such as bead width and thickness (Fig. 4).

Optimizing the process parameters of WAAM is essential for these materials to produce complete and defect-free depositions. Also, high cost and lack of availability of Ni-based alloy wires necessitate its optimal use. Bhuvanesh Kumar et al. [108] have used TS, WFS and voltage as input process parameters keeping 20-mm TSD for depositing Inconel 825. The TS was varied between 3 and 5 m/min, WFS was varied between 3 and 7 m/min, and voltage was varied between 17 and 21 V. The study was carried out to obtain optimal combinations of these parameters to deposit defect-free layers with different bead widths as shown in Fig. 6. The lower bead width of 8.8 mm and the highest bead width of 15.4 mm were obtained within the different levels of input parameters. Another study by Benakis et al. [109] reported the effect of current on the bead geometry of GTAW-WAAM-deposited Inconel 718. Current in different states as main current (I_p), background current (I_b), and delta current (I_D), with different modes such as continuous, slow pulse (low-frequency), inter-pulse (high-frequency), and the combination of both slow pulse and inter-pulse have been applied along with TS and WFS.

The geometrical requirements of weld bead such as width and depth of penetration can be controlled by selecting a suitable level of input current and other parameters. Some examples of Inconel 718 linear weld beads deposited on SS316L substrate based on the parameters combination from design of experiments (DOE) are shown in Fig. 5. The metallographic images of the same weld beads at their cross section are shown in Fig. 6. The bead profiles of the depositions were also varied which lead to different bonding strengths with substrate material.

The deposition method is the other concern that influences the bead geometry and growth of grains. Generally, WAAM uses two different deposition strategies: oscillation path and two-pass multi-layer path, as shown in Fig. 7. A single-pass multi-layer approach is used to fabricate thin walls, whereas the thicker walls require more deposition hence multi-pass strategy is adapted. Mechanical and metallurgical properties of Inconel 625 depositions using these strategies through the CMT-WAAM process are studied by Jiang et al. [75]. Comparatively better mechanical properties and less surface irregularities were found in the two-pass multi-layer path strategy.

The dwell time or interpass time is a period between the completions of successive layers. Dwell time is given for the deposited material to cool down, initiate the grain growth, and avoid residual stresses, distortion, warping, delamination, and other related defects [110]. The advanced WAAM process setups are equipped with different features

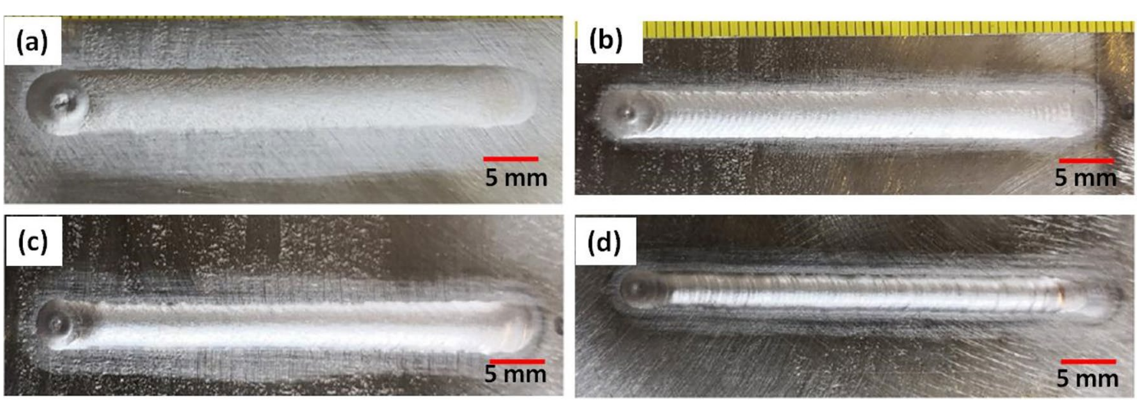

Fig. 5 WAAM-deposited linear weld beads of Inconel 718 at **a** I_p-124 A, I_b-0 A, I_D-0 A, **b** I_p-128 A, I_b-87 A, I_D-0 A, **c** I_p-132 A, I_b-0 A, I_D-78 A and **d** I_p-132 A, I_b-87 A, I_D-50 A (Courtesy of Benakis et al. [109])

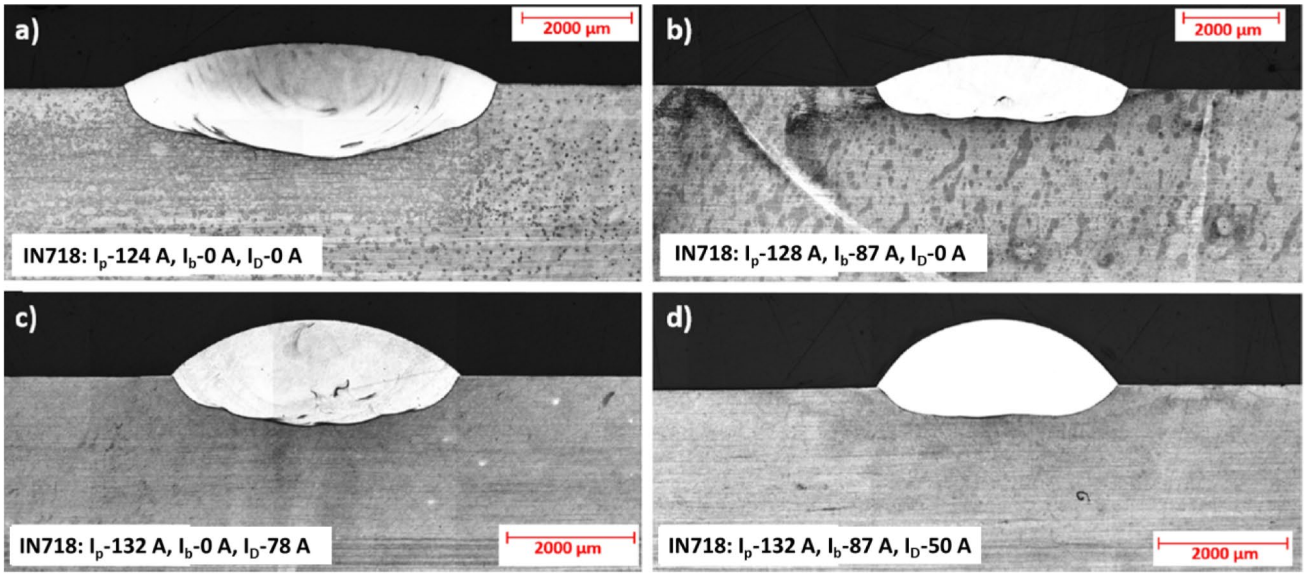

Fig. 6 Metallographic images of Inconel 718 weld beads at their cross section with respect to Fig. 5 (Courtesy of Benakis et al. [109])

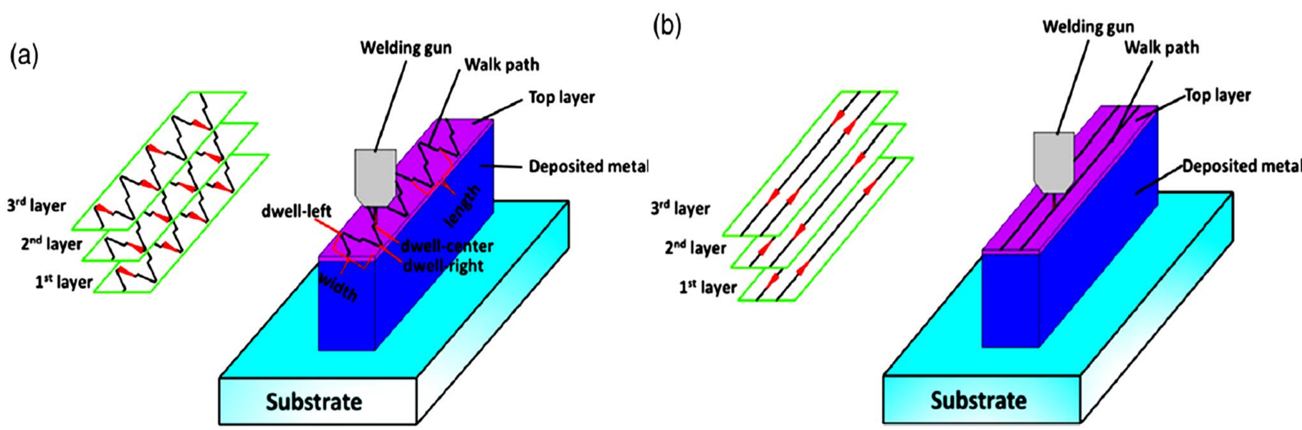

Fig. 7 Metal deposition strategies used in WAAM for thick walls **a** Oscillation path and **b** Two-pass multi-layer path (Courtesy of Jiang et al. [75])

to measure interpass temperature [9, 111], bead geometry [112], and other signals. These advancements aid in-process observations and control to build a quality product. For Ni-based alloys, the previous researchers have used different interpass temperature vary from 80 to 400 °C. For the experimental setups without advanced monitoring and control systems, the researchers used interpass time ranging from 0 to 300 s for Ni-based alloys, as shown in Table 3. Researchers have also tried interpass cold rolling techniques to minimize distortion, residual stresses, and homogeneous material properties [113]. Another method of increasing product quality is a pulsed mode of arc in WAAM. The size of droplets and detachment frequency is controlled by setting an appropriate frequency of the pulse. Compared to continuous depositions, pulsed droplet deposition in WAAM increases physical characteristics and microstructural refinement [114, 115] due to the impact force acts on the molten droplet, as shown in Fig. 8. Additionally, to enable optimized fabrication, the deposition rate and efficiency may be determined by precisely calculating average arc power, linear heat input, and the arc stability index [76].

4.2 Microstructure of WAAMed Ni-based superalloys

The microstructure of Ni-based alloys consists of some intermetallic phases enclosed by a metallic matrix. The most predominant are the matrix gamma (γ) phase, intermetallic precipitate gamma prime (γ'), and the metal carbides. The γ is a solid solution of alloying elements present in Ni, a

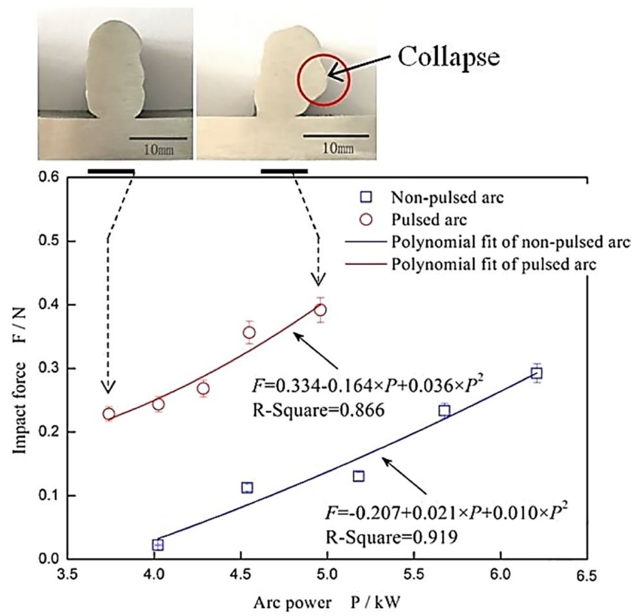

Fig. 8 Comparison of metal deposition and arc force impacts on the droplet between a pulsed arc and non-pulsed arc WAAM (Courtesy of Luo et al. [115])

face-centred-cubic (fcc) austenitic phase. The percentage of γ' phase depends on the elemental composition and the temperature. The γ' phase is primarily responsible for the implausible resistance to creep and the mechanical strength at elevated temperatures. There is another phase called gamma double prime (γ'') with the principal compositions of Ni_3Nb or Ni_3V which is used for strengthening the alloy for a lower temperature range (600–850 °C) since γ' is unstable at this temperature range [116]. Additionally, Ni-based superalloys can show up the other phases such as mu (μ), sigma (σ), and Laves phases at elevated temperatures for an extended duration [117]. The constitute elements which are soluble in the host lattice such as C, Cr, Mo, W, Nb, Ta, Ti and Hf are responsible for the carbide formation, and the formed carbides incline towards precipitations at grain boundaries that can reduce the boundary sliding [118].

Since the WAAM process involves higher operating temperatures during fabrication, it is inevitable to investigate the microstructural evolution. The typical thermal cycle in WAAM consists of repeated heating and cooling [119] which results in inhomogeneous compositions and metastable microstructures. The inhomogeneity in grain growth is majorly identified between adjacent layers of WAAM fabricated parts. However, appropriate cooling strategies can help the formation of homogeneous grain structures. WAAM-deposited Inconel 625 alloys exhibit a columnar dendritic grain structure formed along the build direction which is normal to the deposition direction [103, 105]. A similar grain structure has been noticed in the interlayer interface also. The continuation of columnar grain growth in the layer band is due to the partial remelting of previous layer, as shown in Fig. 9.

The columnar grains were not always parallel to the build direction, but there was a little change in orientation near the melt pool edge. At the centre of deposited walls, the grains are oriented in parallel to the build direction, but few grains inwardly grew to indicate the variation in heat flow near the edges. As shown in Fig. 10, the orientation change shows the remelting region at the interface denoting the boundary. Higher magnification on the depositions confirms the precipitations of γ matrix eutectic phases lined up to the build direction in the interdendritic region. A closer look at the eutectic phase reveals the Laves phase and carbides along with precipitations of TiN particles [76]. There is also a change observed in the shape of Laves phase. The shape varied based on its proximity from the substrate material. For example, Van et al. [78] reported this phenomenon while building Inconel 718 wall using CMT-WAAM process with an interpass cooling time of 30 s. The SEM images show a lamellar-shaped Laves phases majorly. The Laves phases are discrete near the substrate, but they develop continuous phase around the middle portion of the fabricated wall.

Fig. 9 Microstructure of WAAM-deposited Inconel 625 **a** interlayer interface and **b** columnar grain structure (Courtesy of Yangfan et al. [105])

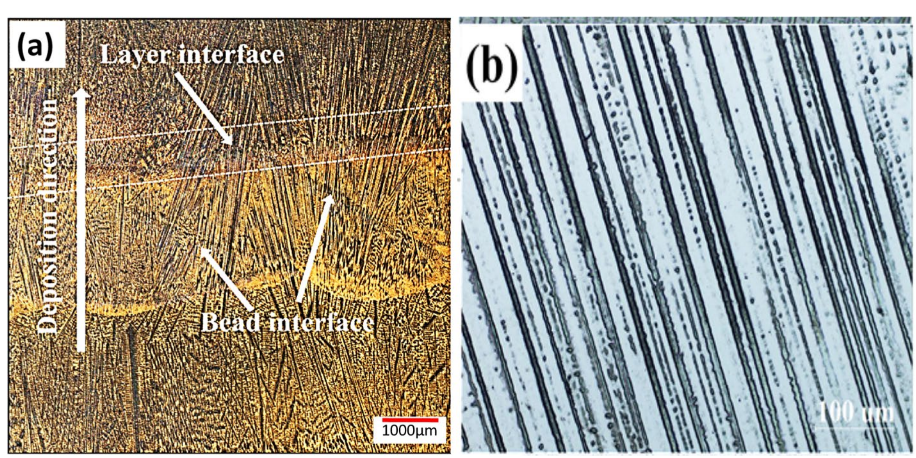

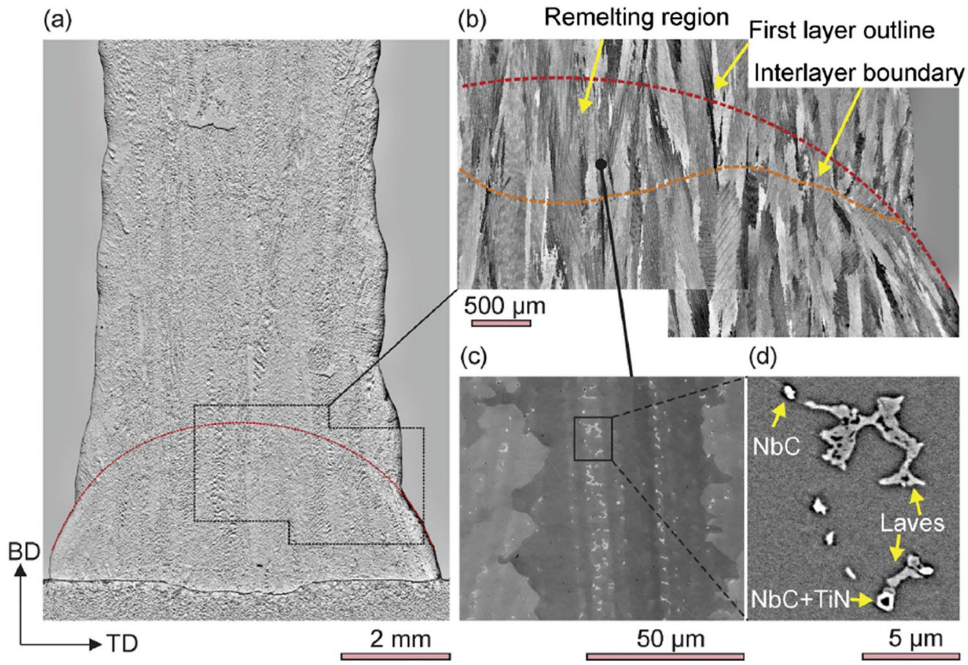

Fig. 10 CMT-WAAM-deposited Inconel 718 **a** macrograph showing the wide linear wall, **b** microstructure showing the orientation of grains near edges, interlayer boundary and remelting region, and (**c** and **d**) eutectic phase γ matrix with the presence of Laves and carbides (Courtesy of Kindermann et al. [76])

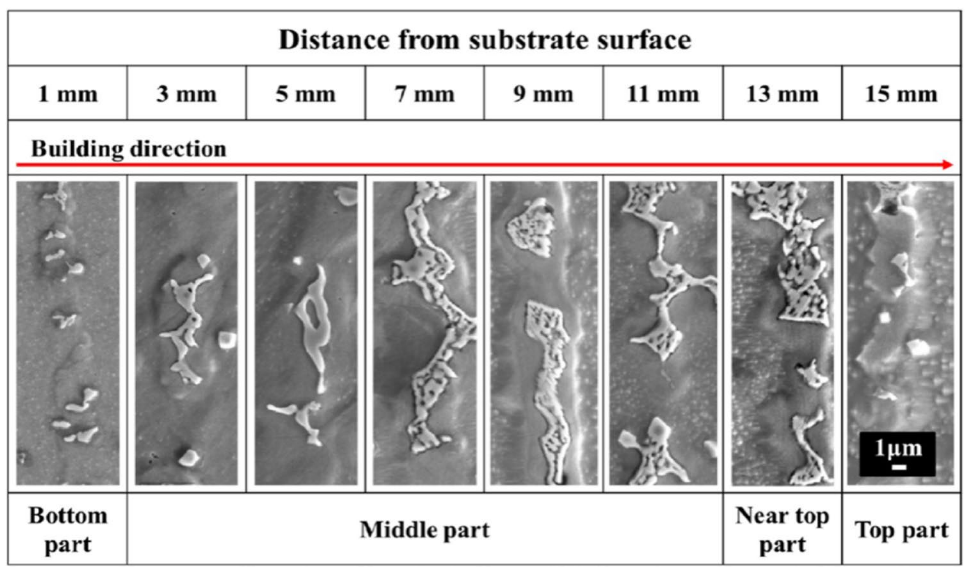

Fig. 11 Microstructural images showing the change in Laves phase shape based on its distance from the substrate in the z-axis build direction (Courtesy of Van et al. [78])

Again at the top of the wall, the discontinuity in Laves phase is observed as shown in Fig. 11. This is mainly due to the effect of cooling rate. Cooling rate is higher at the bottom due to the conduction through substrate and the top due to convective cooling by air/gas supply. It was concluded that prolonging temperature induce the continuous form of Laves phase and higher cooling rates tend to form a discrete Laves phase.

The solidification after deposition is reported to be dendritic, where the interdendritic area is mixed with eutectic elements in the secondary phase. This phenomenon was exhibited in the TIG-WAAM-deposited ATI 817Plus alloy [82] also. The morphology of precipitated particles is reported to be a mixer of μ-phase particles in a plate-like form and strengthening constituents. The micro-segregation during the molten metal solidification forms the Laves phase and the particles of MC carbides. The segregation format is responsible for the formation of precipitates at γ, γ' and μ phases as shown in Fig. 12. Research works have reported a similar microstructural formation in the other Ni-based alloys such as hastelloy [95] and Ni–Cu alloy [107]. The formation of these microstructural features depends on the elemental composition and the process

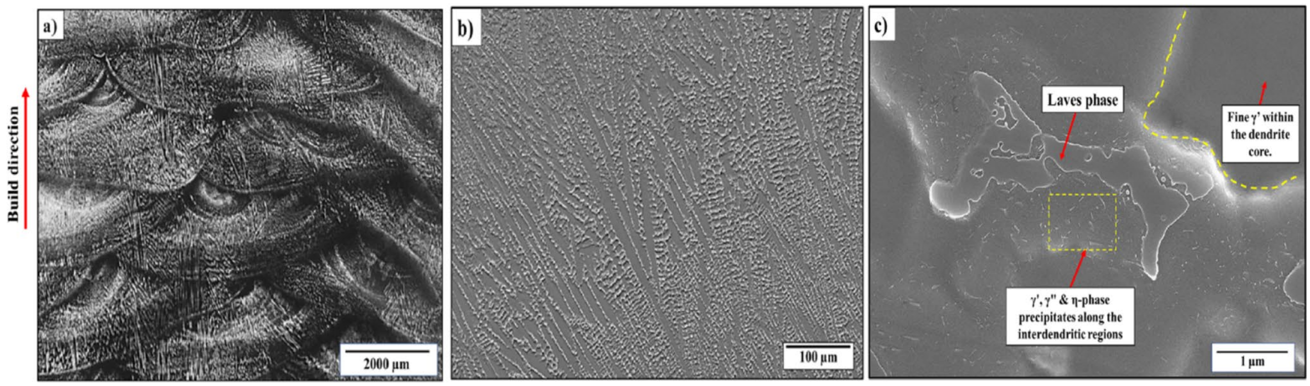

Fig. 12 **a** Microstructural image of as-deposited ATI 718Plus, **b** Microstructure showing the eutectic elements along the interdendritic area in dendritic structure, and **c** γ, γ' and μ phase precipitations (Courtesy of Asala et al. [82])

Table 4 Major mechanical properties of Ni-based superalloys obtained from WAAM process

Materials	Process	Condition	Microstructure	UTS (MPa)	Microhardness	YS (MPa)	El (%)	References
Inconel 625	MIG	AF	Laves + NbC + MC + γ—matrix	696.5	270–285 $HV_{1.0}$	335	46.6	[103]
		SA		670	260–265 $HV_{1.0}$	357.5	59.6	
	CMT	AF	Cellular dendritic structure + coarser dendritic crystal	647.9–687.7	246–259.9 HV	376.9–400.8	43–46.5	[105]
	GTAW	HT	Coarser Laves particles + Nb precipitates	802	240–270 HV	469	42	[121]
	PPAW	IC	Laves phase + NbC carbides	771	285–300 $HV_{0.2}$	480	50	[74]
Inconel 718	CMT-MIG	HT	NbC carbides + TiN inclusions + acicular δ phase	1194	258 ± 9 HV	949	19.9	[77]
	PAAW	AF	Laves + γ phases	872 ± 31	249–277 HV	563 ± 14	34 ± 3	[79]
		HT	Lamellar + γ + δ phases	1152 ± 28	377–436 HV	864 ± 21	23 ± 2	
	GMAW	AF	Nb precipitates + dendritic structure	828 ± 8	266 ± 21 HV	473 ± 6	28 ± 2	[122]
Ni–Ti	GTAW	AF	Coarse B2 grains + lenticular precipitates	927.9	–	–	8.7	[91]
	TIG	AF	Austenite, martensite, R-phase + Ni–Ti precipitates	571.4 ± 18.6	228–245 HV	350	16.8 ± 2.4	[88]
	GTAW	AF	Ni–Ti precipitates + dendrite structure	–	700–820 $HV_{0.2}$	–	–	[89]
Hastelloy	GTAW	AF	Ni, Mo precipitates + columnar dendrites	399 ± 12[a] 469 ± 52[b]	200–215 $HV_{0.1}$	186 ± 27[a] 287 ± 50[b]	43 ± 6[a] 55 ± 3[b]	[95]
	GMAW	AF	Columnar and equiaxed grains + parallel dendrites	680.73	–	311.08	28–35	[96]
Monel K500	CMT	HT	Coarse Ti–rich particles	622 ± 20	265 HV	280 ± 3	31 ± 1	[107]
FM60			Coarse Mn-rich particles	428 ± 20	173 HV	190 ± 5	40 ± 2	

AF As-fabricated, *SA* Solution annealed, *IC* Interpass cooling, HT: heat-treated

[a]In build direction

[b]Perpendicular to build direction

parameters that attribute to the superior level performance of Ni-based superalloys. The observation with respect to resulting microstructure and the formation of precipitates from the deposition of different Ni-based alloys using WAAM are shown in Table 4.

4.3 Mechanical properties

Most researchers attempted to investigate the microstructural and mechanical characteristics of WAAM-deposited Ni-based alloy samples cut from wall-shaped multi-layer depositions rather than functional components. Majority of the mechanical properties experimentally investigated are the ultimate tensile strength (UTS), yield strength (YS), elongation (El), and microhardness. The detailed mechanical properties resulted from WAAM fabricated samples of different Ni-based superalloys are shown in Table 4. While WAAM fabricated samples show compatible mechanical properties with wrought form, some post-fabrication heat treatments have proven to improve some properties due to microstructural changes [120].

Majority of the research works revealed the improved mechanical properties of Ni-based alloys after WAAM deposition compared to wrought material. As-fabricated samples showed coarser dendrites with the presence of lesser Mo, and Nb precipitates at some points. These secondary elements responsible for strengthening were absorbed during precipitation and lead to reduced mechanical properties [105]. The microstructures were dominated by columnar dendrites and showed relatively less microhardness and tensile properties [88, 95]. Heat-treated samples of Ni-based alloys showed Ni–Ti, and carbides with a lamellar, and acicular phases and improved mechanical properties [77, 91, 98, 123].

Very few research works have reported inferior mechanical properties of WAAM depositions compared to as-cast or wrought material properties [5, 103]. But the data from majority of the articles demonstrate the improvements due to post-deposition strengthening strategies like solution annealing, interpass cooling, and heat treatment. Wear resistance is also an important property required for functional applications, and few articles have investigated it. Wang et al. [89] systematically analysed the wear resistance of WAAM-deposited NiTi coatings on Ti6Al4V substrate. The dry sliding wear tests revealed that the wear rates of NiTi surfaces varied between 3.611×10^{-4} and 3.948×10^{-4} mm^3/Nm with a load of 5N. But the wear rates were decreased with an increased load of 10N. However, the NiTi coatings offered 60–70% higher wear resistance than the substrate material.

Similarly, Marenych et al. [98] investigated the wear properties of heat-treated WAAM depositions of Monel K500 and FM60. The particle density due to heat treatment of up to 610 °C in the first ageing has increased the wear resistance in both the materials. But the second phase of heat treatment with 480 °C resulted in the particle growth and minor variations only. Conclusively, heat treatments have improved the wear properties of Monel K500 to about 16%, whereas FM60 has experienced a 24% improvement. The comparison of wear resistance in terms of mass loss between Monel K500 and FM60 after heat treatment is portrayed in Fig. 13. Thorough investigations on these aspects are essentially needed to characterize the wear properties of Ni-based superalloys.

Although the studies related to the fatigue properties are very limited in the literature, few have applied fatigue tests on WAAM processed metals. This may be because of

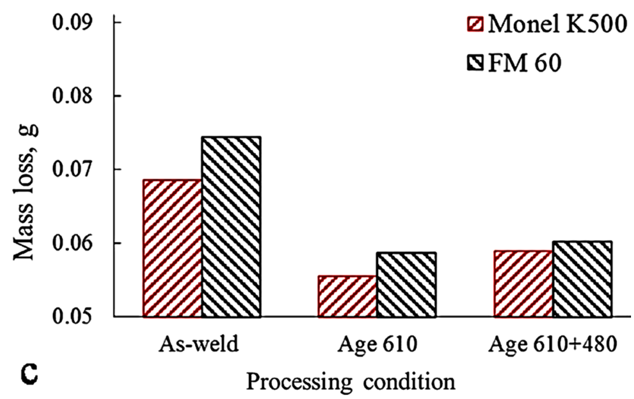

Fig. 13 Variation in mass loss (to predict wear resistance) of heat-treated WAAM depositions of Monel K500 and FM60 (Courtesy of Marenych et al. [98])

the duration of fatigue test. A fatigue test measuring the fatigue strength analogous to a fatigue life of a component for 10^7 cycles with a frequency of 10 Hz can consume nearly 12 days [124]. Apart from other metals, fatigue properties of Ni-based alloys processed by WAAM are still countable in numbers. Rajesh Kannan et al. [96] have investigated the fatigue resistance of defect-free hastelloy C-276 deposited over a SS 904L wall using GMAW-based WAAM process. After the cyclic loading test, the WAAMed hastelloy C-276 sustained 2×10^6 cycles and showed a fatigue resistance of 156 MPa which is 28–35% lower than wrought specimen. Also, microstructural defects can influence the fatigue resistance of WAAMed components. Siddiqui and Araiza [125] have investigated the effect of microstructural defects on the torsional fatigue resistance of WAAMed Inconel 718. The torsional fatigue fracture occurred where the un-melted particles and lack of fusion appeared. Furthermore, the correlation between build orientation-reliant fracture mechanics and torsional fatigue failure was made by the author. But post-processing heat treatments were reported to improve the fatigue properties of WAAMed Ni-based alloys similar to other metals. Yet the investigations to analyse the fatigue properties of WAAMed Ni-based alloys must be conducted in future.

4.4 Heat treatment effects

Heat treatment processes are usually carried out as a post-deposition process to alter the surface properties. Altering the surface properties is aimed to suit specific application environments. But the main purpose of heat treatment on WAAM-deposited Ni-based alloy parts is to overcome one of the inevitable challenges in metal AM viz. anisotropy [38]. This post-heat treatment process on Ni-based alloys mainly alters the built parts' microstructure resulting in improved mechanical properties.

The anisotropy in Inconel 718 is attributed to the development of columnar grain growth and fibre textures. The Laves phase present in as-fabricated Inconel 718 deteriorates the mechanical performances; therefore, it requires additional heat treatment processes. Seow et al. [126] introduced two different heat treatment conditions, namely standard homogeneous and solution aged (HSA), and modified homogeneous and aged (HA) to WAAM-deposited Inconel 718. The results were appreciable as shown in Fig. 14. The modified HA was more effective than standard HAS. The HA dissolved the Laves phase without any δ precipitates, but not in the case of HAS or ageing only as shown in Fig. 15. Thus, the Inconel 718 after modified HA yields higher elongation properties both at room and elevated temperatures (650 °C) [127]. Table 5 shows the mechanical performances of WAAM-Inconel 718 subjected to different heat treatments

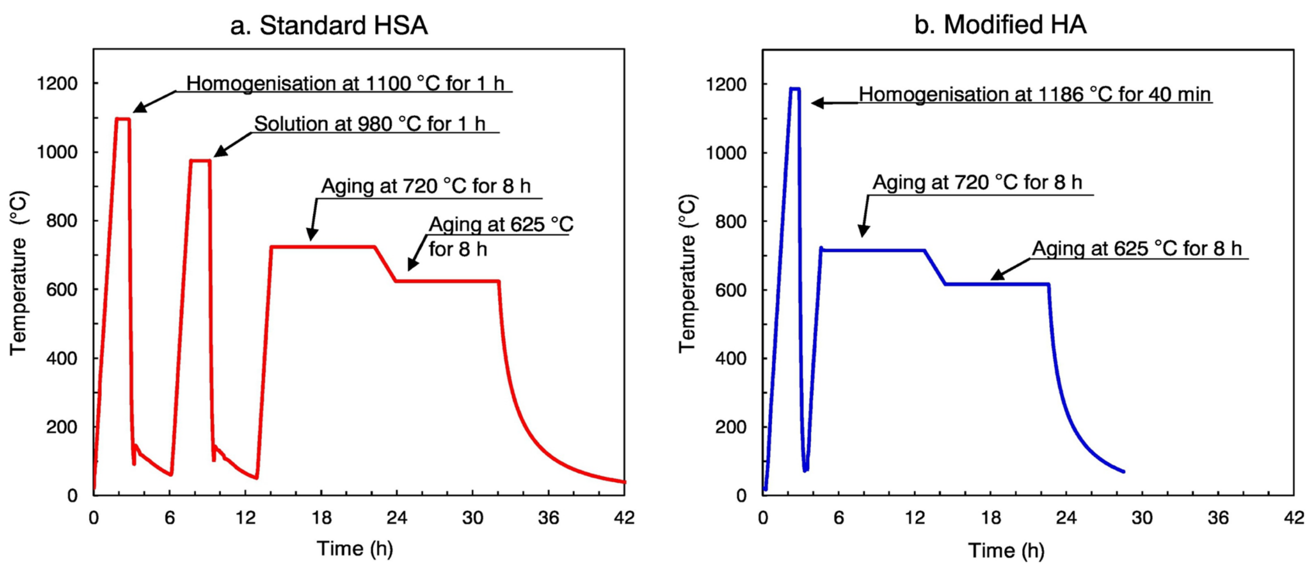

Fig. 14 Two different heat treatment conditions employed on WAAM-Inconel 718 (Courtesy of Seow et al. [127])

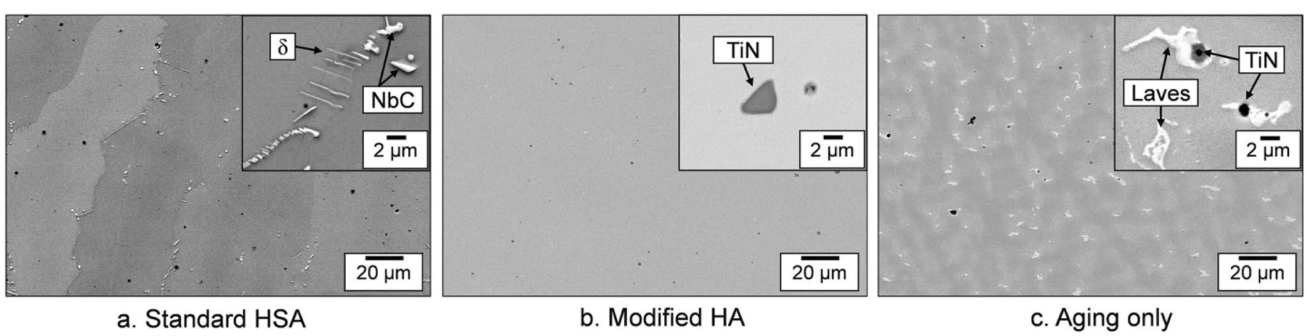

Fig. 15 Backscatter electron microscopic images of heat-treated WAAMed Inconel 718 after **a** Standard HSA, **b** Modified HA and **c** Ageing only (Courtesy of Seow et al. [127])

Table 5 Mechanical performances of WAAMed Inconel 718 subjected to different heat treatments

	Room temperature				Elevated temperature (650 °C)	
	As-fabricated	Ageing only	Standard HSA	Modified HA	As-fabricated	Modified HA
UTS (MPa)	750	1070	1120	1040	630	820
YS (MPa)	430	950	1060	860	400	730
EL (%)	21	2	0.9	20	9	6.7

Values rounded to the nearest tenth

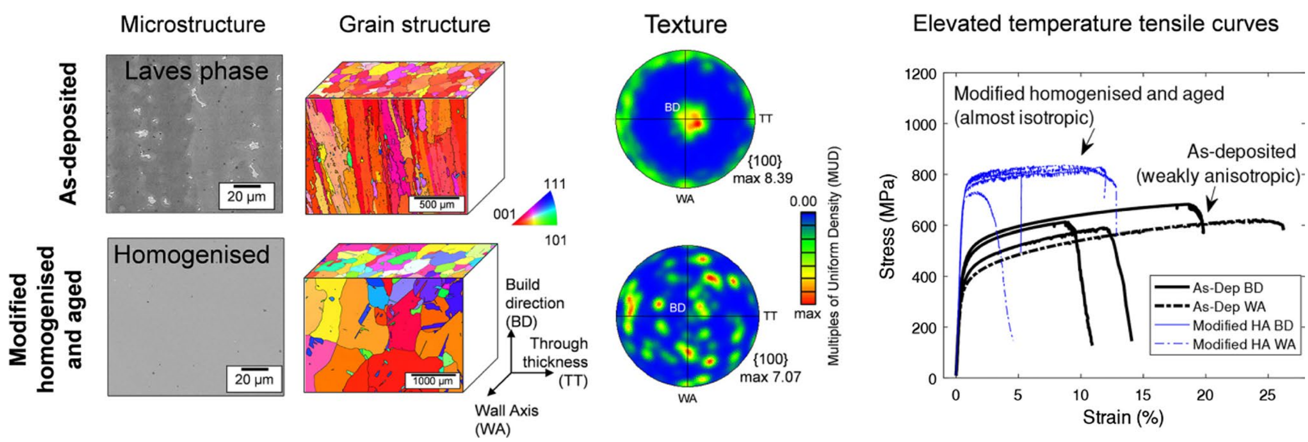

Fig. 16 Effect of post-heat treatment on WAAMed Inconel 718 (Courtesy of Seow et al. [127])

[127]. The effect of post-heat treatment is shown in Fig. 16. The modified HA offers almost the isotropic behaviour of the material.

Inconel 625, after heat-treated at 980 °C, eliminated the Laves phases without altering the grain structure. But prolonged exposure to such an environment resulted in an increase in δ-phases and the size of metal carbides [104]. It was also found the κ_{II} phases control the tensile properties of WAAMed Inconel 625. Two-hour heat-treated samples developed superior tensile characteristics due to the elimination of the Laves phases. However, significant changes in microhardness values were not found [128]. After WAAMed Inconel 625 was introduced to 1100 °C heat treatment for 6 h, the Laves phases were dissolved next to the secondary phases, and new equiaxed grains in *xy* plane were grown. The grains elongated along the dendrite direction in *xz* plane. Yet, it is reported that anisotropy cannot be eradicated completely [129].

A standard heat treatment process [130] on the WAAMed ATI 718Plus resulted in degradation of tensile properties due to excessive formation of η-phase particles and traces of partially dissolved Laves phases. A modified homogeneous heat treatment process involves 1075 °C for 1 h and is then reduced to 950 °C for 40 min and finally at 788 °C for 8 h as the stage 1 process. The stage 2 process had the same constituent, the only difference being the initial homogeneous heat treatment involved 1150 °C for 1 h and 950 °C for 6 h, followed by the same furnace cooling as stage 1 [131]. TEM results of the post-deposition heat-treated WAAMed ATI 718Plus using this modified heat treatment process showed a reduction in η phases. Results also showed the strengthening precipitates (γ' phases) without increment in γ'' phases, which escalates the strength of the material [81].

Hastelloy C276 fabricated using WAAM was subjected to post-fabrication heat treatment at 871 °C. Results showed the higher strength due to Mo-rich nano-sized μ phase formation but compromising the ductility, while the same material heat-treated at 1177 °C did not show μ phase precipitates, thereby increased the strength and lowered the anisotropy [132]. Shen et al. [90] subjected the WAAM-deposited $Ni_{53}Ti_{47}$ binary alloy to a post-fabrication heat treatment and evaluated its microstructure using a neutron diffraction experiment. During this study, at a rate of 2 °C/min, the temperature of the WAAMed $Ni_{53}Ti_{47}$ is raised to 1050 °C and held for 10 min; see Fig. 17. During this stage, the hcp-lattices are transformed to bcc lattices. The temperature is brought down to 200 °C at a rate of 2 °C/min and then at room temperature in a vacuum chamber filled with helium gas. This heat treatment process had reduced the residual stress produced during fabrication. Also, this heat treatment has generated the Ni_4Ti_3 phase precipitates evenly which attribute to significant improvement in mechanical properties. Moreover, the c/a ratio (lattice parameters) variation was helpful in the accurate detection of the phase transformation process [90]. Thus, the heat treatment process in WAAM-deposited Ni-based alloys has a significant effect in overcoming the anisotropy character. It also has a considerable impact on increasing mechanical properties.

4.5 Corrosion behaviour

Corrosion behaviour is an essential property for the applications under aggressive circumstances. Ni-based alloys are well-known for their superior corrosion resistance property at higher temperatures but may reduce during downtimes due to room temperature corrosion [133]. Hence, it is worthwhile to investigate the corrosion resistance of WAAMed Ni-based alloys. Zhang and Ojo [106] investigated the corrosion resistance of heat-treated Inconel 718 fabricated using TIG-WAAM process. Several analysis methods like potentiodynamic polarization, electrochemical impedance spectroscopy (EIS), X-ray photoelectron spectroscopy (XPS)

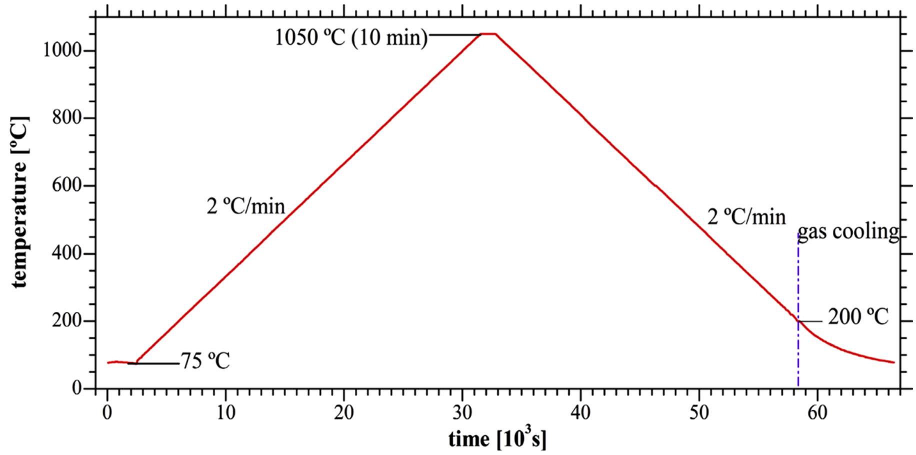

Fig. 17 Heat treatment process for WAAM-$Ni_{53}Ti_{47}$ binary alloy (Courtesy of Shen et al. [90])

Table 6 Comparison of corrosion resistance characteristics between HT-WAAM and HT-wrought Inconel 718 samples (Courtesy of Zhang and Ojo [106])

Solution	Specimen	i_{corr} (μA/cm²)	E_{corr} (mV)	i_{crit} (μA/cm²)	i_{pass} (μA/cm²)	E_{pp} (mV)	Passive range ΔE_{pass} (mV)
HNO_3	HT-WAAM	16.0 ± 0.7	471.5 ± 1.5	523 ± 31	421 ± 57	708 ± 6.3	756 ± 1.3
	HT-wrought	11.6 ± 0.8	510 ± 8.5	66 ± 2.9	27.6 ± 4.9	590 ± 6.1	850 ± 5.4
H_2SO_4	HT-WAAM	3.89 ± 0.1	371.67 ± 38	541 ± 11.7	251 ± 37	678 ± 3.2	808 ± 3.5
	HT-wrought	2.80 ± 0.4	400.67 ± 56	83.1 ± 3.5	22.7 ± 7.6	555 ± 6.8	891 ± 6.3

analysis, and potentiostatic polarization have been performed to compare the corrosion behaviour of HT-WAAM and HT-wrought Inconel 718 samples. Different acidic solutions such as HNO_3 and H_2SO_4 of each 1 M have been used for the potentiodynamic polarization analysis. Using the electrochemical parameters such as corrosion current density (i_{corr}), critical current density (i_{crit}), corrosion potential (E_{corr}), passivation current density (i_{pass}), and passivation potential (ΔE_{pass}), the corrosion behaviour was analysed.

The formation of passive layers offers corrosion resistance during electrochemical studies in Ni-based alloys [134, 135]. Lower i_{pass} denotes the higher formation of passive layers resulting in higher corrosion resistance. But HT-WAAM samples have shown higher i_{pass} (nearly ten times higher) than HT-wrought samples, indicating the WAAM samples possess significantly less corrosion resistance than wrought samples. Similarly, other parameters have their influencing patterns on the electrochemical measurements. Conclusively, WAAM specimens have shown lesser corrosion resistance property in both the HNO_3 and H_2SO_4 solutions, as shown in Table 6. The nature of passivation layer formation was examined using XPS analysis. This method was used to inspect the chemical compositions which are responsible for passive layer formation. The XPS spectra have detected the peaks of Ni 2*p*, Cr 2*p*, O 1*s*, C 1*s*, Mo 3*d*, Nb 3*d*, and Fe 2*p*, as shown in Fig. 18. The elements like Cr_2O_3 and MoO_3 are

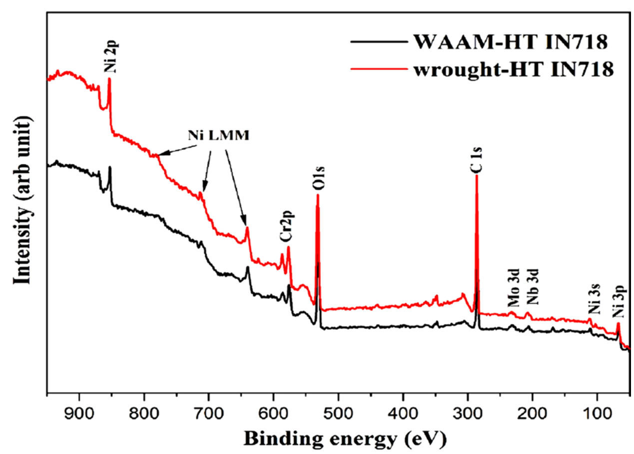

Fig. 18 XPS spectra after the potentiostatic polarization on HT-WAAM and HT-wrought specimens (Courtesy of Zhang and Ojo [106])

usually dense and offer more passive protection against corrosion. The presence of these protective elements is higher in wrought samples than WAAM fabricated pieces which again confirmed the lesser corrosive resistance property of WAAMed specimens.

Asala et al. [83] investigated the hot corrosion performance of WAAM-deposited ATI 718plus. The low melting eutectic of sodium vanadate was prepared at temperatures as low as 500 °C. The test specimens were heated up to 160 °C, and the prepared salt was sprayed on it to a required quantity. Further, the coated samples were exposed to isothermal oxidation inside the alumina crucible at around 650–705 °C for different hours. Then, the weights, microstructure, and elemental compositions were analysed and compared with the values before exposure. The oxidation attack was found to be uniform in the wrought specimen, but notable changes were identified around the dendritic core regions. After a broader analysis of the specimens, it was concluded that the hot corrosion resistance of WAAM-deposited samples are slightly low compared to the wrought specimen. The same procedure of testing for standard heat-treated (STA) and homogenization treated (HTA) samples revealed that the HTA samples exhibited higher hot corrosion resistance than the STA samples. On the whole, corrosion resistance behaviour after heat treatment was not improved than wrought one. Still, the investigations on corrosion resistance of WAAM depositions for different materials under this class need to be performed.

4.6 Defects

Though WAAM offers a wide range of advantages concerning new product development and many design freedoms, the process is associated with defects whose dynamics are yet to be studied. Since WAAM follows the arc welding principle, it is inherent to the defects of fusion welding processes like porosity, residual stresses, distortions, and deformities [38]. These defects are highly dependent on the material alloys used and the parameters employed for layered deposition. Product quality and its performance are directly proportional to the type and nature of defects. Path programming, process modelling, and online control of process control the product quality parameters [136]. Table 7 provides the consolidated report on the research works carried out in understanding the defects evolved during WAAM of Ni-based alloys.

4.6.1 Residual stress

Residual stress occurs mainly due to the Laves phases present in the as-fabricated alloys and the reasons for which have been extensively discussed in earlier sections. It is found that the residual stresses are reduced by increasing the welding speed [137], which is the case for WAAM. During substrate heating, the selective growth behaviour of grains has influenced the residual stresses that accounts for constrain effects in the WAAM of $Ni_{52}Ti$ [138]. Distortions results from the residual stresses [37], which also prevail in the fabrication of Ni-based alloys. The effects of residual stress have their highest effect during

Table 7 Summary of research works carried out in analysing the defects of WAAMed Ni-based alloys

Ni-based alloy	Defects identified/studied						Inspection methods	Treatment methods	Effects	References
	Residual stress	Distortion	Porosity	Delamination	Cracks	Others				
Ni52Ti	✓	✓	–	✓	–	–	TEM	Substrate heating	Reduced defects	[138]
NiTi SMA	✓	✓	–	–	–	Melt-pool instability	XRD	Pre-surface treatment	Reduced defects	[92]
IN718	–	–	✓	–	✓	Centreline grain boundary	SEM	Input energy control	Reduced defects	[139]
Hastelloy X	–	–	✓	–	–	–	SEM	Optimization (one-way ANNOVA)	Zero defects	[94]
IN718	–	–	–	–	✓	–	NDT	–	–	[141]
Ni-rich NiTi SMA	–	–	✓	✓	✓	Oxide inclusions	SEM, XRD	–	Zero defects	[88]
IN718	–	–	✓	–	–	Oxide inclusions	SEM	Post-fabrication heat treatment	Zero defects	[146]
IN625	–	–	✓	–	✓	–	SEM	–	Zero defects	[105]
Hastelloy C276	–	–	✓	✓	✓	Micro-voids	TEM, XRD	–	Zero defects	[132]

the fabrication of thin walls. However, these defects can be treated by hybridizing the WAAM process using pre-heating the deposition surface through laser markings [92].

4.6.2 Porosity

Porosity is an insufficient penetration of deposited metal between the gaps over the preceding layers. Porosity during WAAM of IN718 occurs due to unfavourable energy input and welding speed. Volumetric energy inputs below 14 J/mm^3 and above 35 J/mm^3 have resulted in porosity defects. Within this window of energy input along with a speed of 3 mm/s, the WAAMed IN718 had reduced porosity [139]. It is evident that porosity results in deterioration of tensile properties. Upon studying the porosity effects over fatigue strength of WAAM- Ti–6Al–4 V using Kitagawa–Takahashi diagram, it was found that 100-μm-diameter pores are predicted to be more critical [140]. In WAAMed Hastelloy X, the radial flow of the weld pool at the bead centre has contributed towards the generation of voids (interfacial defects) as shown in Fig. 19. Employing one-way ANOVA, the process parameters were optimized to ensure the absence of interfacial regions, thus avoiding interfacial defects. However, printing path strategies did not influence the porosity [94]. The internal defects were identified using an ultrasonic testing method and confirmed using metallographic analysis. It was reported that a large weld pool might result in internal defects.

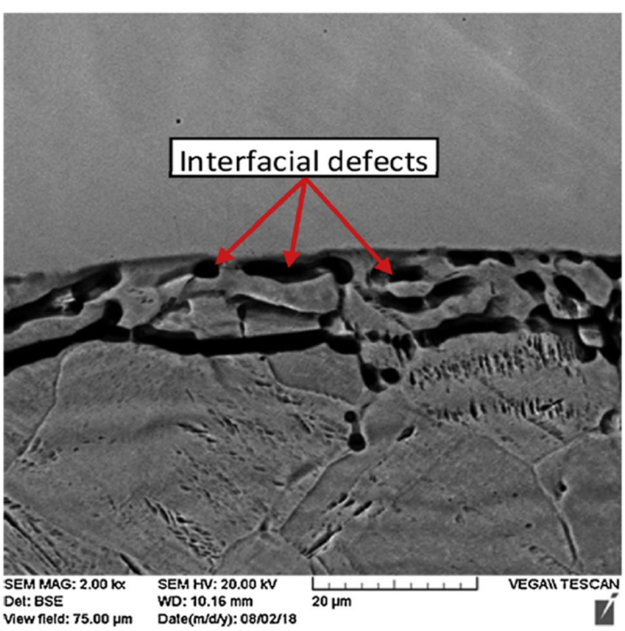

Fig. 19 Porosity in the interface areas of WAAMed hastelloy X (Courtesy of Dinovitzer et al. [94])

4.6.3 Delamination

Delamination is the process of one layer slipping upon another due to poor bonding during deposition. During fabrication of WAAM-$Ni_{52}Ti$ that intended for 30 layers of deposit using in situ alloying without substrate heating, the process experienced severe delamination right after five layers. Heating the substrate prior to metal deposition is recommended to overcome delamination [138]. Figure 20 shows the back scattered electron (BSE) and TEM-black field (BF) images of grains at different substrate heated conditions of WAAMed Ni-rich NiTi alloy.

The cause for delamination is the residual stresses resulted from dilution effect. The various sizes of NiTi precipitates with lenticular shape and high aspect ratios were found in the precipitate morphologies. These precipitates intersect each other by approximately 60° as shown in Fig. 20. This behaviour accounts for constrain effect due to residual stresses. Coarsening of these precipitates is found while increasing the substrate heating temperature resulting in decreased stresses and has avoided the delamination defect.

4.6.4 Cracks

The phenomenon of cracking happens in two forms: solidification and liquation. Solidification cracking usually originates from low plasticity (ductility) and tensile stresses in transverse directions. At the same time, liquation cracking emerges due to moving heat sources. During fabrication of IN718, both these cracking occurs due to the eutectic reaction, which forms the Laves phases at 1200 °C [139]. It was found that these defects are anisotropic and attributed to reduced toughness. It was also observed that the crack orientation has much influence over the mechanical properties [141]. Figure 21 shows the crack and associated Laves phase in WAAM-IN718. Micro-cracks were identified during the fracture analysis of WAAMed Ni-rich NiTi shape memory alloy (SMA) which has occurred due to nucleation of voids. However, the effects of micro-cracks on fabricated material's performance were negligible [88].

Artaza et al. [142] investigated the influence of heat input on hot cracking while fabricating Inconel 718 using PAW-based WAAM process. Two different cooling strategies were adapted, namely ICS and controlled overlay strategy (COS) for fabrication. The SEM micrographs of samples made through both strategies showed the presence of precipitates. The precipitates of ICS samples were Laves and Ti, Nb-rich inclusions and further identified to be MC carbides. These enrichments affect the microstructure and resulted in the formation of cracks. Compared to COS strategy, the ICS samples experienced low thermal gradient and lead to faster solidification. Hence, the

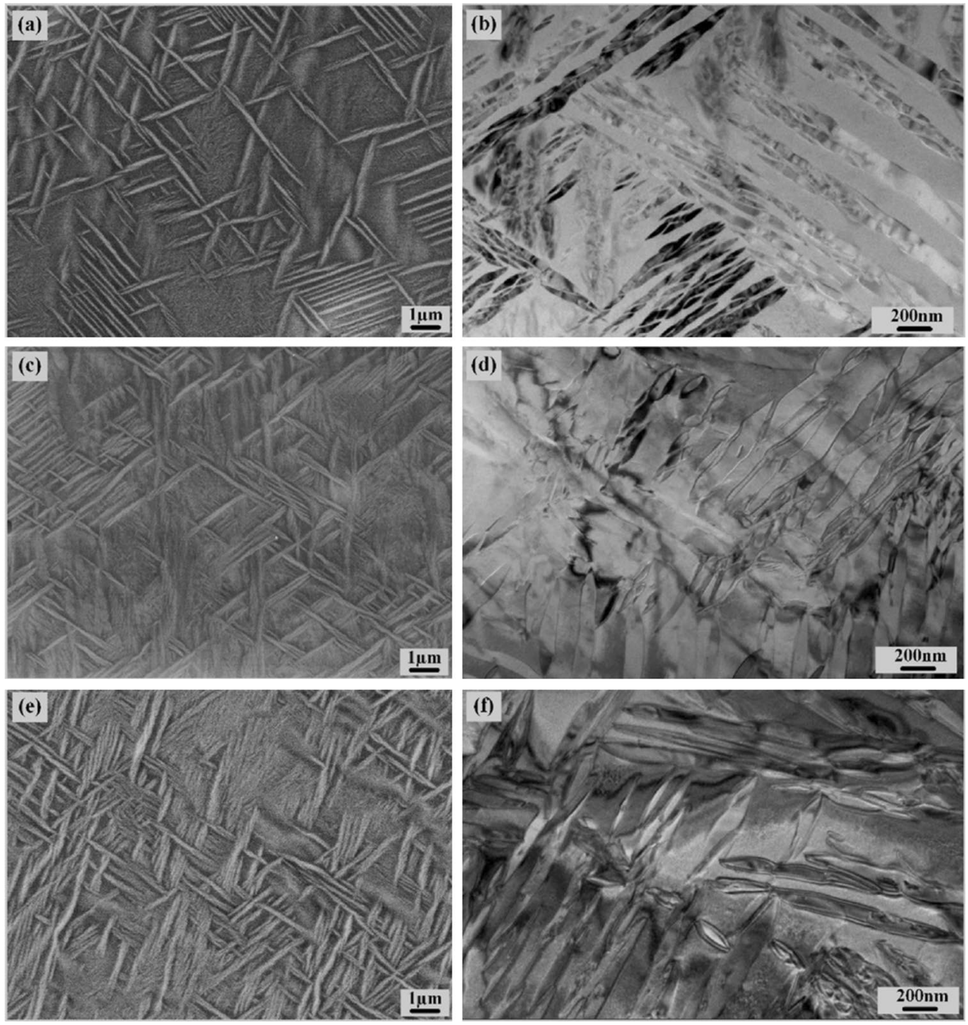

Fig. 20 BSE and TEM-BF images of grains at different substrate heated conditions **a** and **b** 150 °C, **c** and **d** 250 °C, and **e** and **f** 350 °C (Courtesy of Wang et al. [138])

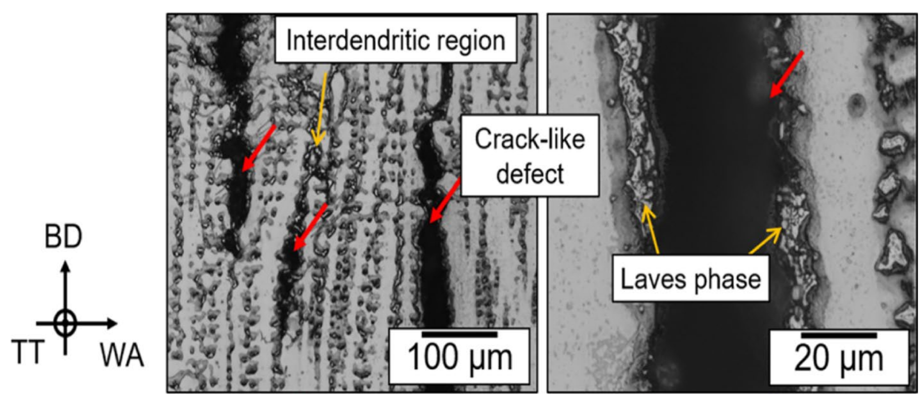

Fig. 21 SEM images of cracks in WAAM-IN718 along with Laves phase bonded to the defect boundaries (Courtesy of Seow et al. [141])

microstructure showed more homogeneous with discontinuous cracks as shown in Fig. 22. In case of COS samples, due to longer solidification time, the needle-like precipitates including Laves phase appeared. From XRD analysis, the phase was identified to be δ-phase and its occurrence is completely based on manufacturing process parameters, and solidification time. The needle-like precipitates in interdendritic regions developed continuous cracks; see Fig. 22. The cracks were reported to be resulting from liquation cracking [143]. This phenomenon initially develops around the undissolved nitrides or carbide precipitates in the heat-affected zone (HAZ). The formation of Laves

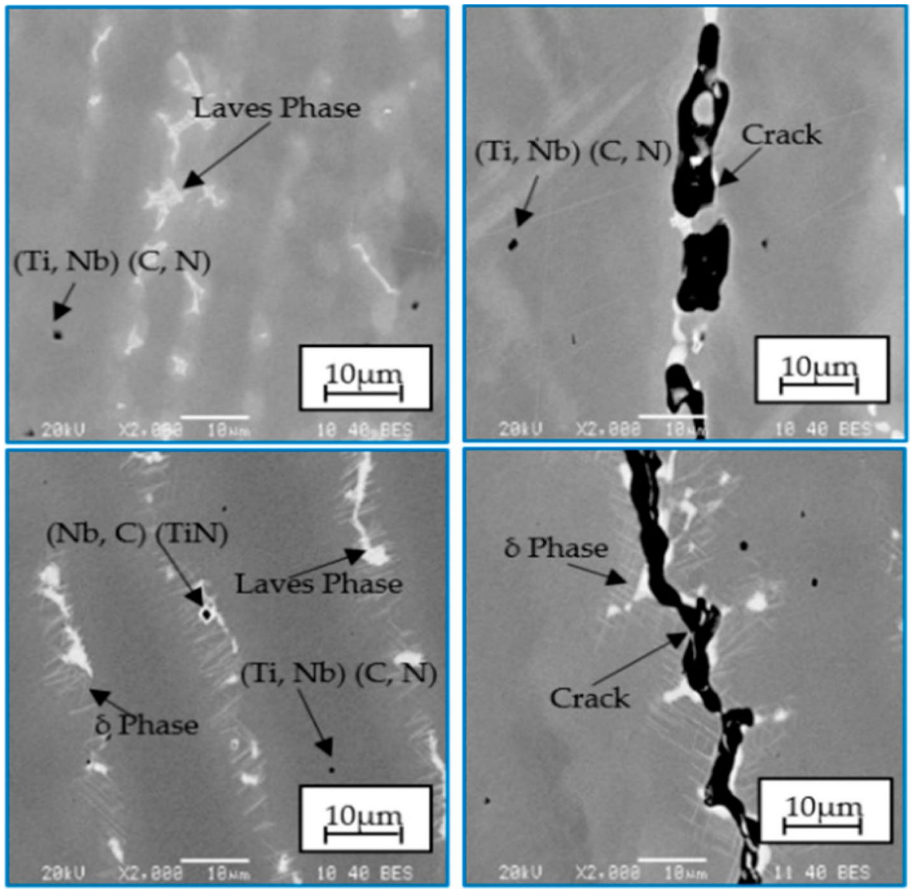

Fig. 22 Hot cracking during PAW-WAAM of Inconel 718 using **a** and **b** ICS strategy, and **c** and **d** COS strategy (Courtesy of Artaza et al. [142])

phase due to eutectic reaction under 1200 °C led to the initiation of cracking since Laves phase is brittle [144].

4.6.5 Summary on the defects

In addition to the previously discussed defects, few welding related defects may prone to appear in WAAMed Ni-based alloys. These defects include inclusions, centreline grain boundary, lack of fusion voids, collapsing and un-melted wires sticking to the deposits [94, 145]. The inclusions are mostly in the form of oxides. However, oxide inclusions have occasional effects on the mechanical properties of the WAAMed Ni-based alloys [146]. The centreline grain boundary formed during the fabrication of WAAMed IN718 has a considerable impact on the materials' mechanical performance and can be averted by controlling the input energy [139]. Still more research works need to be carried out to investigate in detail about these defects arising from WAAM of Ni-based alloys. The summary of research works carried out to investigate the defects of WAAMed Ni-based alloys is shown in Table 7. Major defects reported by most of the research works include the porosity and cracks. The presence of residual stresses, distortion, and the occurrence of delamination were found less than the major defects. Post-fabrication heat treatment processes were highly influencing in eliminating the defects. Though many of the defects can be completely eradicated, residual stress and distortion defects were only reduced to the minimum possible extend by heat treatment processes [138].

5 Challenges and limitations

Although the WAAM process is becoming more and more emerging topic around the world due to its benefits, such as the capability of fabricating large parts with adequate structural complexity, high deposition rates, and the processability of a wide range of metallic materials [147], there exist some challenges and limitations associated with the fabrication of Ni-based alloys. The challenges and limitations that hamper the application of WAAM on Ni-based alloys are as follow:

1. The microstructure and mechanical properties of WAAM-deposited Ni-based alloys show inhomogeneity along the build direction due to different heat transfer mechanisms.

2. Since Ni-based alloys possess high melting temperature, deciding upon the parameters such as interpass cooling time and temperature is a real-time challenge. Also, a higher level of heat input imparted on the substrate and build part for the entire fabrication duration leads to the distortion. Handling it without the generation of residual stress is a highly challenging task.
3. Though inclusions of impurities are lesser than the other MAM processes, its presence during the interpass cooling periods being the cause for defects in WAAMed Ni-based alloys and controlling it is a highly demanding task.
4. The elements which offer passive protection against corrosion such as Cr_2O_3 and MoO_3 were less in WAAMed Ni-based alloys compared to wrought material. Post-heat-treatment processes did not show any notable improvements on the corrosion behaviour.

Apart from these property-specific challenges, there exist a few basic challenges associated with the fabrication of WAAMed Ni-based alloys. Shortage of reliable and integrated real-time monitoring and controlling systems limits the controlled depositions of Ni-based alloys. The lack of availability of different Ni-based alloy wires with the required dimensions and forms (machine-winded reel without physical defects) limits the research works to be in fewer numbers. Handling stiff wires of superior grades of Ni-based alloys is also a little difficult task. Avoiding the occurrence of spattering due to mismatched parameter levels is challenging, and it requires extensive attention for fabricating Ni-based alloys using WAAM. Repairing of functional components using WAAM is further limits its application. This is mainly due to the dimensionally imprecise fabrication. Standardizing the process in terms of process parameters and post-deposition heat treatment conditions for different materials, deposition geometries and required properties may highly contribute to minimize the current limitations of WAAM.

6 Conclusion and future scope

The WAAM process is a comparatively low-cost and high-speed deposition technology for the fabrication of large components. The WAAM process substitutes the powder-based DED processes with complete usage efficiency but can handle moderate product complexity. Additionally, due to lower surface area per unit volume, the inclusion of impurities is minimized. From the detailed literature review, the following conclusion can be drawn in favour of processing Ni-based alloys using WAAM:

1. The costs of different grades of Ni-based materials are significantly low in wire form compared to powder form used by DED. The WAAM process, due to less waste, convenient machine setup, deposition rate, and build time, is an effective, efficient, and economical alternative to other metal AM processes offering a better BTF ratio.
2. WAAM processes involve higher input energy and varying heat transfer mechanisms which leads to inhomogeneous characteristics of deposited materials. The application of short-circuit-based WAAM technique like CMT-MIG and CMT-TIG are more or less equally competent techniques in reducing the heat input during fabrication. Hence, they are highly suitable for processing high-temperature materials like Ni-based alloys.
3. The resulting microstructures majorly consist of dendritic grains mixed with eutectic elements in the secondary phase. These elements were reported to be the precipitates of Laves phase and MC carbides. But the size, orientation, and distribution were varied in different locations of depositions. This anisotropic phenomenon is the major cause for inhomogeneous mechanical properties at different locations of the depositions.
4. Post-processing heat treatments on WAAM-deposited Ni-based alloy parts improves the microstructural attributes resulting in better and homogeneous mechanical properties.
5. Comparing to UTS, YS, hardness, and El of conventionally manufactured wrought Ni-based alloys, WAAM-deposited components exhibit improved mechanical properties. In addition, heat treatment processes improves the wear-resistant property also. But both as-deposited and heat-treated WAAMed Ni-based alloys possess slightly reduced corrosion resistance property compared to wrought material.

There are many possible ways by which the WAAM process can be incorporated into multi-disciplinary research that integrates different areas such as thermo-mechanical engineering and electro-mechanics. Similarly, integrating the conventional machining process with WAAM analogous to ultrasonic AM can produce more complex structures with the finest surface finish.

6.1 Future research directions

Since the research works related to the fabrication of Ni-based alloys using WAAM are significantly less in the literature, future research works can be propagated in many directions including,

1. Only a countable number of articles have performed wear and corrosion studies on WAAMed Ni-based

alloys. More studies in future should attempt to explore the surface characteristics of WAAMed Ni-based alloys.
2. The investigations were mainly included the UTS, YS, El, and hardness properties alone. But future studies can be performed to investigate the fatigue properties of WAAMed nickel alloys.
3. Optimization of process parameters for different bead geometry and the correlation between different substrate materials with Ni-based alloys are the other area to be focused by future studies.
4. Fabrication of very thin walls with good dimensional accuracy using WAAM is the present-day requirement. Also, more variants in Ni alloy is required to be investigated for the applicability of WAAM process.

Funding This work was supported by the National Institute of Technology, Tiruchirappalli.

Declarations

Conflict of interest There are no potential conflict of interest to disclose.

References

1. Laureijs RE, Roca JB, Narra SP, Montgomery C, Beuth JL, Fuchs ER (2017) Metal additive manufacturing: cost competitive beyond low volumes. J Manuf Sci Eng 139:081010-1–081010-9
2. Bhuvanesh Kumar M, Sathiya P (2021) Methods and materials for additive manufacturing: a critical review on advancements and challenges. Thin-Walled Struct 159:107228. https://doi.org/10.1016/j.tws.2020.107228
3. Varatharaj Kannan S, Yogasundar ST, Suraj Singh R, Tamilarasu S, Bhuvanesh Kumar M (2014) Rapid prototyping of human implants with case study. Int J Innov Res Sci Eng Technol 3:6
4. Williams SW, Martina F, Addison AC, Ding J, Pardal G, Colegrove P (2016) Wire+ arc additive manufacturing. Mater Sci Technol 32:641
5. Derekar KS (2018) A review of wire arc additive manufacturing and advances in wire arc additive manufacturing of aluminium. Mater Sci Technol 34:895. https://doi.org/10.1080/02670836.2018.1455012
6. Thapliyal S (2019) Challenges associated with the wire arc additive manufacturing (WAAM) of aluminum alloys. Materials Research Express 6:112006
7. Korzhyk V, Khaskin V, Voitenko O, Sydorets VN, Dolianovskaia O (2017) Welding technology in additive manufacturing processes of 3d objects. Mater Sci Forum 906:121–130
8. Rodrigues TA, Duarte V, Miranda RM, Santos TG, Oliveira JP (2019) Current status and perspectives on wire and arc additive manufacturing (WAAM). Materials 12:1121
9. Ding J, Colegrove P, Mehnen J et al (2011) Thermo-mechanical analysis of wire and arc additive layer manufacturing process on large multi-layer parts. Comput Mater Sci 50:3315. https://doi.org/10.1016/j.commatsci.2011.06.023
10. Wu B, Ding D, Pan Z et al (2017) Effects of heat accumulation on the arc characteristics and metal transfer behavior in wire arc additive manufacturing of Ti_6Al_4V. J Mater Process Technol 250:304
11. Frazier WE (2014) Metal additive manufacturing: a review. J Mater Eng Perform 23:1917
12. Horgar A, Fostervoll H, Nyhus B, Ren X, Eriksson M, Akselsen O (2018) Additive manufacturing using WAAM with AA5183 wire. J Mater Process Technol 259:68
13. Gu J, Ding J, Williams SW et al (2016) The strengthening effect of inter-layer cold working and post-deposition heat treatment on the additively manufactured Al–6.3 Cu alloy. Mater Sci Eng A 651:18
14. Wang T, Zhang Y, Wu Z, Shi C (2018) Microstructure and properties of die steel fabricated by WAAM using H13 wire. Vacuum 149:185
15. Müller J, Grabowski M, Müller C et al (2019) Design and parameter identification of wire and arc additively manufactured (WAAM) steel bars for use in construction. Metals 9:725
16. Zhuo Y, Yang C, Fan C et al (2021) Grain refinement of wire arc additive manufactured titanium alloy by the combined method of boron addition and low frequency pulse arc. Mater Sci Eng, A 805:140557
17. Alonso U, Veiga F, Suárez A, Artaza T (2020) Experimental investigation of the influence of wire arc additive manufacturing on the machinability of titanium parts. Metals 10:24
18. Gneiger S, Österreicher JA, Arnoldt AR, Birgmann A, Fehlbier M (2020) Development of a high strength magnesium alloy for wire arc additive manufacturing. Metals 10:778
19. Guo Y, Pan H, Ren L, Quan G (2019) Microstructure and mechanical properties of wire arc additively manufactured AZ80M magnesium alloy. Mater Lett 247:4. https://doi.org/10.1016/j.matlet.2019.03.063
20. Seow CE, Zhang J, Coules HE et al (2020) Effect of crack-like defects on the fracture behaviour of wire + arc additively manufactured nickel-base alloy 718. Addit Manuf 36:101578
21. Lan B, Wang Y, Liu Y et al (2021) The influence of microstructural anisotropy on the hot deformation of wire arc additive manufactured (WAAM) Inconel 718. Mater Sci Eng, A 823:141733
22. Li Y, Polden J, Pan Z et al (2021) A defect detection system for wire arc additive manufacturing using incremental learning. J Ind Inf Integr 27:100291
23. Ding D, Pan Z, Van Duin S, Li H, Shen C (2016) Fabricating superior NiAl bronze components through wire arc additive manufacturing. Materials 9:652
24. Hassel T, Carstensen T (2020) Properties and anisotropy behaviour of a nickel base alloy material produced by robot-based wire and arc additive manufacturing. Weld World 64:1921
25. Bhujangrao T, Veiga F, Suárez A, Iriondo E, Mata FG (2020) High-temperature mechanical properties of IN718 alloy: comparison of additive manufactured and wrought samples. Crystals 10:689
26. Kok Y, Tan XP, Wang P et al (2018) Anisotropy and heterogeneity of microstructure and mechanical properties in metal additive manufacturing: a critical review. Mater Des 139:565
27. Haghdadi N, Laleh M, Moyle M, Primig S (2021) Additive manufacturing of steels: a review of achievements and challenges. J Mater Sci 56:64
28. Tan JHK, Sing SL, Yeong WY (2020) Microstructure modelling for metallic additive manufacturing: a review. Virtual Phys Prototyp 15:87
29. Köhler M, Fiebig S, Hensel J, Dilger K (2019) Wire and arc additive manufacturing of aluminum components. Metals 9:608
30. Jinoop A, Paul C, Bindra K (2019) Laser-assisted directed energy deposition of nickel super alloys: a review. Proc Inst Mech Eng Part L J Mater Design Appl 233:2376

31. Yin Y, Tan Q, Bermingham M, Mo N, Zhang J, Zhang M-X (2021) Laser additive manufacturing of steels. Int Mater Rev 67(5):487–573
32. Zhang LC, Liu Y, Li S, Hao Y (2018) Additive manufacturing of titanium alloys by electron beam melting: a review. Adv Eng Mater 20:1700842
33. Sui Y, Zorman CA (2020) Inkjet printing of metal structures for electrochemical sensor applications. J Electrochem Soc 167:037571
34. Gujba AK, Medraj M (2020) Power ultrasonic additive manufacturing: process parameters, microstructure, and mechanical properties. Adv Mater Sci Eng 2020:1064870. https://doi.org/10.1155/2020/1064870
35. Norrish J, Polden J, Richardson I (2021) A review of wire arc additive manufacturing: development, principles, process physics, implementation and current status. J Phys D Appl Phys 54:473001. https://doi.org/10.1088/1361-6463/ac1e4a
36. Chaturvedi M, Scutelnicu E, Rusu CC, Mistodie LR, Mihailescu D, Subbiah AV (2021) Wire arc additive manufacturing: review on recent findings and challenges in industrial applications and materials characterization. Metals 11:939
37. Wu B, Pan Z, Ding D et al (2018) A review of the wire arc additive manufacturing of metals: properties, defects and quality improvement. J Manuf Process 35:127. https://doi.org/10.1016/j.jmapro.2018.08.001
38. Dhinakaran V, Ajith J, Fathima Yasin Fahmidha A, Jagadeesha T, Sathish T, Stalin B (2020) Wire arc additive manufacturing (WAAM) process of nickel based superalloys: a review. Mater Today Proc 21:920. https://doi.org/10.1016/j.matpr.2019.08.159
39. Li Z, Cui Y, Wang L et al (2022) An investigation into Ti-22Al-25Nb in-situ fabricated by electron beam freeform fabrication with an innovative twin-wire parallel feeding method. Addit Manuf 50:102552. https://doi.org/10.1016/j.addma.2021.102552
40. Ma Y, Cuiuri D, Hoye N, Li H, Pan Z (2015) The effect of location on the microstructure and mechanical properties of titanium aluminides produced by additive layer manufacturing using in-situ alloying and gas tungsten arc welding. Mater Sci Eng A 631:230
41. Ayarkwa K, Williams SW, Ding J (2017) Assessing the effect of TIG alternating current time cycle on aluminium wire+ arc additive manufacture. Addit Manuf 18:186
42. Xiong J, Zhang G (2014) Adaptive control of deposited height in GMAW-based layer additive manufacturing. J Mater Process Technol 214:962
43. Posch G, Chladil K, Chladil H (2017) Material properties of CMT—metal additive manufactured duplex stainless steel blade-like geometries. Weld World 61:873
44. Tian Y, Shen J, Hu S, Wang Z, Gou J (2019) Microstructure and mechanical properties of wire and arc additive manufactured Ti-6Al-4V and AlSi5 dissimilar alloys using cold metal transfer welding. J Manuf Process 46:337
45. Pang J, Hu S, Shen J, Wang P, Liang Y (2016) Arc characteristics and metal transfer behavior of CMT+ P welding process. J Mater Process Technol 238:212
46. Fang X, Zhang L, Li H, Li C, Huang K, Lu B (2018) Microstructure evolution and mechanical behavior of 2219 aluminum alloys additively fabricated by the cold metal transfer process. Materials 11:812
47. Rosli NA, Alkahari MR, MFb Abdollah, S Maidin, FR Ramli, SG Herawan, (2021) Review on effect of heat input for wire arc additive manufacturing process. J Market Res 11:2127. https://doi.org/10.1016/j.jmrt.2021.02.002
48. Spaniol E, Ungethüm T, Trautmann M, Andrusch K, Hertel M, Füssel U (2020) Development of a novel TIG hot-wire process for wire and arc additive manufacturing. Weld World 64:1329. https://doi.org/10.1007/s40194-020-00871-w
49. Vimal K, Srinivas MN, Rajak S (2021) Wire arc additive manufacturing of aluminium alloys: a review. Mater Today Proc 41:1139
50. Balasubramanian K, Senthilkumar V (2020) Additive manufacturing applications for metals and composites. IGI Global, United States of America
51. Zhang C, Li Y, Gao M, Zeng X (2018) Wire arc additive manufacturing of Al-6Mg alloy using variable polarity cold metal transfer arc as power source. Mater Sci Eng A 711:415. https://doi.org/10.1016/j.msea.2017.11.084
52. Wang P, Hu S, Shen J, Liang Y, Pang J (2016) Effects of electrode positive/negative ratio on microstructure and mechanical properties of Mg/Al dissimilar variable polarity cold metal transfer welded joints. Mater Sci Eng A 652:127
53. Singh S, Sharma SK, Rathod DW (2021) A review on process planning strategies and challenges of WAAM. Mater Today Proc 47:6564:6575
54. Zahid M, Hai K, Khan M, Shekha A, Pervaiz S, Ali SM, Abdul-Latif O, Salman M (2020) Wire arc additive manufacturing (waam): reviewing technology, mechanical properties, applications and challenges. In: ASME international mechanical engineering congress and exposition. American Society of Mechanical Engineers, United States of America
55. Byun J-G, Cho S-M (2016) Trend of metal 3D printing by welding. J Weld Join 34:1
56. Cheepu M, Lee CI, Cho SM (2020) Microstructural characteristics of wire arc additive manufacturing with Inconel 625 by super-TIG welding. Trans Indian Inst Metals 73:1475–1479
57. Lin JJ, Lv YH, Liu YX et al (2016) Microstructural evolution and mechanical properties of Ti-6Al-4V wall deposited by pulsed plasma arc additive manufacturing. Mater Des 102:30. https://doi.org/10.1016/j.matdes.2016.04.018
58. Yaseer A, Chen H (2021) A review of path planning for wire arc additive manufacturing (WAAM). J Adv Manuf Syst 20(3):589–609
59. Wang X, Wang A, Li Y (2019) A sequential path-planning methodology for wire and arc additive manufacturing based on a water-pouring rule. Int J Adv Manuf Technol 103:3813
60. Ma G, Zhao G, Li Z, Xiao W (2019) IOP conference series: materials science and engineering. IOP Publishing, Bristol
61. Ding D, Pan Z, Cuiuri D, Li H (2015) A practical path planning methodology for wire and arc additive manufacturing of thin-walled structures. Robot Comput Integr Manuf 34:8
62. Jafari D, Vaneker TH, Gibson I (2021) Wire and arc additive manufacturing: Opportunities and challenges to control the quality and accuracy of manufactured parts. Mater Design 202:109471
63. Singh CP, Sarma R, Kapil S (2022) The qualitative analysis of warpage on residual stresses in wire arc additive manufacturing. Mater Today Proc 62:6619. https://doi.org/10.1016/j.matpr.2022.04.615
64. Szost BA, Terzi S, Martina F et al (2016) A comparative study of additive manufacturing techniques: residual stress and microstructural analysis of CLAD and WAAM printed Ti–6Al–4V components. Mater Des 89:559. https://doi.org/10.1016/j.matdes.2015.09.115
65. Xiong J, Zhang Y, Pi Y (2020) Control of deposition height in WAAM using visual inspection of previous and current layers. J Intell Manuf 32:2209–2217
66. Kozamernik N, Bračun D, Klobčar D (2020) WAAM system with interpass temperature control and forced cooling for near-net-shape printing of small metal components. Int J Adv Manuf Technol 110:1955
67. Xia C, Pan Z, Polden J et al (2020) A review on wire arc additive manufacturing: Monitoring, control and a framework of automated system. J Manuf Syst 57:31

68. Wang Y, Xu X, Zhao Z et al (2021) Coordinated monitoring and control method of deposited layer width and reinforcement in WAAM process. J Manuf Process 71:306
69. Tang S, Wang G, Zhang H (2019) In situ 3D monitoring and control of geometric signatures in wire and arc additive manufacturing. Surf Topogr Metrol Prop 7:025013
70. Michel F, Lockett H, Ding J, Martina F, Marinelli G, Williams S (2019) A modular path planning solution for wire + arc additive manufacturing. Robot Comput Integr Manuf 60:1. https://doi.org/10.1016/j.rcim.2019.05.009
71. Pollock TM, Tin S (2006) Nickel-based superalloys for advanced turbine engines: chemistry, microstructure and properties. J Propul Power 22:361
72. Chamanfar A, Jahazi M, Gholipour J, Wanjara P, Yue S (2011) Mechanical property and microstructure of linear friction welded WASPALOY. Metall Mater Trans A 42:729
73. Dinda GP, Dasgupta AK, Mazumder J (2009) Laser aided direct metal deposition of Inconel 625 superalloy: microstructural evolution and thermal stability. Mater Sci Eng A 509:98. https://doi.org/10.1016/j.msea.2009.01.009
74. Xu FJ, Lv YH, Xu BS, Liu YX, Shu FY, He P (2013) Effect of deposition strategy on the microstructure and mechanical properties of Inconel 625 superalloy fabricated by pulsed plasma arc deposition. Mater Des 45:446. https://doi.org/10.1016/j.matdes.2012.07.013
75. Jiang Q, Zhang P, Yu Z et al (2021) Microstructure and mechanical properties of thick-walled Inconel 625 alloy manufactured by wire arc additive manufacture with different torch paths. Adv Eng Mater 23:2000728
76. Kindermann RM, Roy MJ, Morana R, Prangnell PB (2020) Process response of Inconel 718 to wire + arc additive manufacturing with cold metal transfer. Mater Design 195:109031. https://doi.org/10.1016/j.matdes.2020.109031
77. Xu X, Ding J, Ganguly S, Williams S (2019) Investigation of process factors affecting mechanical properties of INCONEL 718 superalloy in wire + arc additive manufacture process. J Mater Process Technol 265:201. https://doi.org/10.1016/j.jmatprotec.2018.10.023
78. Van D, Dinda GP, Park J, Mazumder J, Lee SH (2020) Enhancing hardness of Inconel 718 deposits using the aging effects of cold metal transfer-based additive manufacturing. Mater Sci Eng A 776:139005. https://doi.org/10.1016/j.msea.2020.139005
79. Wang K, Liu Y, Sun Z, Lin J, Lv Y, Xu B (2020) Microstructural evolution and mechanical properties of Inconel 718 superalloy thin wall fabricated by pulsed plasma arc additive manufacturing. J Alloys Compd 819:152936. https://doi.org/10.1016/j.jallcom.2019.152936
80. Asala G, Khan AK, Andersson J, Ojo OA (2017) Microstructural analyses of ATI 718Plus® produced by wire-ARC additive manufacturing process. Metall Mater Trans A 48:4211. https://doi.org/10.1007/s11661-017-4162-2
81. Oguntuase O, Ojo OA, Beddoes J (2020) Influence of post-deposition heat treatments on the microstructure and mechanical properties of wire-arc additively manufactured ATI 718Plus. Metall Mater Trans A 51:1846. https://doi.org/10.1007/s11661-019-05619-w
82. Asala G, Andersson J, Ojo OA (2019) Analysis and constitutive modelling of high strain rate deformation behaviour of wire–arc additive-manufactured ATI 718Plus superalloy. Int J Adv Manuf Technol 103:1419. https://doi.org/10.1007/s00170-019-03616-2
83. Asala G, Andersson J, Ojo OA (2019) Hot corrosion behaviour of wire-arc additive manufactured Ni-based superalloy ATI 718Plus®. Corros Sci 158:108086. https://doi.org/10.1016/j.corsci.2019.07.010
84. Li B, Shen Y, An Q (2020) Structural origin of reversible martensitic transformation and reversible twinning in NiTi shape memory alloy. Acta Mater 199:240
85. Fang C, Yam MC, Ma H, Chung KF (2015) Tests on superelastic Ni–Ti SMA bars under cyclic tension and direct-shear: towards practical recentring connections. Mater Struct 48:1013
86. Zhang Q, Hao S, Liu Y et al (2020) The microstructure of a selective laser melting (SLM)-fabricated NiTi shape memory alloy with superior tensile property and shape memory recoverability. Appl Mater Today 19:100547. https://doi.org/10.1016/j.apmt.2019.100547
87. Wang J, Pan Z, Yang G, Han J, Chen X, Li H (2019) Location dependence of microstructure, phase transformation temperature and mechanical properties on Ni-rich NiTi alloy fabricated by wire arc additive manufacturing. Mater Sci Eng A 749:218. https://doi.org/10.1016/j.msea.2019.02.029
88. Zeng Z, Cong BQ, Oliveira JP et al (2020) Wire and arc additive manufacturing of a Ni-rich NiTi shape memory alloy: microstructure and mechanical properties. Addit Manuf 32:101051. https://doi.org/10.1016/j.addma.2020.101051
89. Wang J, Pan Z, Wang L et al (2020) In-situ dual wire arc additive manufacturing of NiTi-coating on Ti6Al4V alloys: microstructure characterization and mechanical properties. Surf Coatings Technol 386:125439. https://doi.org/10.1016/j.surfcoat.2020.125439
90. Shen C, Reid M, Liss K-D et al (2020) In-situ neutron diffraction study on the high temperature thermal phase evolution of wire-arc additively manufactured $Ni_{53}Ti_{47}$ binary alloy. J Alloys Compd 843:156020. https://doi.org/10.1016/j.jallcom.2020.156020
91. Wang J, Pan Z, Wang Y et al (2020) Evolution of crystallographic orientation, precipitation, phase transformation and mechanical properties realized by enhancing deposition current for dual-wire arc additive manufactured Ni-rich NiTi alloy. Addit Manuf 34:101240. https://doi.org/10.1016/j.addma.2020.101240
92. Singh S, Resnina N, Belyaev S et al (2021) Investigations on NiTi shape memory alloy thin wall structures through laser marking assisted wire arc based additive manufacturing. J Manuf Process 66:70. https://doi.org/10.1016/j.jmapro.2021.04.004
93. Bharat Kumar CH, Anandakrishnan V (2020) Experimental investigations on the effect of wire arc additive manufacturing process parameters on the layer geometry of Inconel 825. Mater Today Proc 21:622. https://doi.org/10.1016/j.matpr.2019.06.727
94. Dinovitzer M, Chen X, Laliberte J, Huang X, Frei H (2019) Effect of wire and arc additive manufacturing (WAAM) process parameters on bead geometry and microstructure. Addit Manuf 26:138
95. Qiu Z, Wu B, Zhu H et al (2020) Microstructure and mechanical properties of wire arc additively manufactured Hastelloy C276 alloy. Mater Design 195:109007. https://doi.org/10.1016/j.matdes.2020.109007
96. Rajesh Kannan A, Mohan Kumar S, Pravin Kumar N, Siva Shanmugam N, Vishnu AS, Palguna Y (2020) Process-microstructural features for tailoring fatigue strength of wire arc additive manufactured functionally graded material of SS904L and Hastelloy C-276. Mater Lett 274:127968. https://doi.org/10.1016/j.matlet.2020.127968
97. Marenych O (2019) School of mechanical, materials, mechatronic and biomedical engineering. University of Wollongong, Australia
98. Marenych O, Kostryzhev A, Shen C, Pan Z, Li H, van Duin S (2019) Precipitation strengthening in Ni–Cu alloys fabricated using wire arc additive manufacturing technology. Metals 9:105
99. Elahinia M, Shayesteh Moghaddam N, Taheri Andani M, Amerinatanzi A, Bimber BA, Hamilton RF (2016) Fabrication of NiTi through additive manufacturing: a review. Prog Mater Sci 83:630. https://doi.org/10.1016/j.pmatsci.2016.08.001

100. Bhuvanesh Kumar M, Sathiya P, Parameshwaran R (2020) Parameters optimization for end milling of Al7075–ZrO_2–C metal matrix composites using GRA and ANOVA. Trans Indian Inst Met. https://doi.org/10.1007/s12666-020-02089-2
101. Kumar MB, Parameshwaran R, Deepandurai K, Senthil SM (2020) Influence of milling parameters on surface roughness of Al–SiC–B4C composites. Trans Indian Inst Met. https://doi.org/10.1007/s12666-020-01960-6
102. Cunningham CR, Flynn JM, Shokrani A, Dhokia V, Newman ST (2018) Invited review article: strategies and processes for high quality wire arc additive manufacturing. Addit Manuf 22:672. https://doi.org/10.1016/j.addma.2018.06.020
103. Ravi G, Murugan N, Arulmani R (2020) Microstructure and mechanical properties of Inconel-625 slab component fabricated by wire arc additive manufacturing. Mater Sci Technol 36:1785. https://doi.org/10.1080/02670836.2020.1836737
104. Tanvir ANM, Ahsan MRU, Ji C, Hawkins W, Bates B, Kim DB (2019) Heat treatment effects on Inconel 625 components fabricated by wire + arc additive manufacturing (WAAM)—part 1: microstructural characterization. Int J Adv Manuf Technol 103:3785. https://doi.org/10.1007/s00170-019-03828-6
105. Yangfan W, Xizhang C, Chuanchu S (2019) Microstructure and mechanical properties of Inconel 625 fabricated by wire-arc additive manufacturing. Surf Coat Technol 374:116. https://doi.org/10.1016/j.surfcoat.2019.05.079
106. Zhang LN, Ojo OA (2020) Corrosion behavior of wire arc additive manufactured Inconel 718 superalloy. J Alloys Compd 829:154455. https://doi.org/10.1016/j.jallcom.2020.154455
107. Marenych OO, Kostryzhev AG, Pan Z, Li H, van Duin S (2019) Comparative effect of Mn/Ti solute atoms and TiC/Ni_3(Al, Ti) nano-particles on work hardening behaviour in NiCu alloys fabricated by wire arc additive manufacturing. Mater Sci Eng A 753:262. https://doi.org/10.1016/j.msea.2019.03.040
108. Bhuvanesh Kumar M, Sathiya P, Rajesh Kannan G, Karthikeyan M (2022) Investigation on the microstructure and microhardness of Inconel 825 thick wall fabricated by wire arc additive manufacturing. Mater Lett 317:132115. https://doi.org/10.1016/j.matlet.2022.132115
109. Benakis M, Costanzo D, Patran A (2020) Current mode effects on weld bead geometry and heat affected zone in pulsed wire arc additive manufacturing of Ti-6-4 and Inconel 718. J Manuf Process 60:61. https://doi.org/10.1016/j.jmapro.2020.10.018
110. Mukherjee T, Zhang W, DebRoy T (2017) An improved prediction of residual stresses and distortion in additive manufacturing. Comput Mater Sci 126:360. https://doi.org/10.1016/j.commatsci.2016.10.003
111. Zhang S, Li J, Kou H, Yang J, Yang G, Wang J (2016) Effects of thermal history on the microstructure evolution of Ti-6Al-4V during solidification. J Mater Process Technol 227:281. https://doi.org/10.1016/j.jmatprotec.2015.08.030
112. Xiong J, Yin Z, Zhang W (2016) Closed-loop control of variable layer width for thin-walled parts in wire and arc additive manufacturing. J Mater Process Technol 233:100. https://doi.org/10.1016/j.jmatprotec.2016.02.021
113. Colegrove PA, Donoghue J, Martina F, Gu J, Prangnell P, Hönnige J (2017) Application of bulk deformation methods for microstructural and material property improvement and residual stress and distortion control in additively manufactured components. Scripta Mater 135:111. https://doi.org/10.1016/j.scriptamat.2016.10.031
114. Guo J, Zhou Y, Liu C, Wu Q, Chen X, Lu J (2016) Wire arc additive manufacturing of AZ31 magnesium alloy: grain refinement by adjusting pulse frequency. Materials 9:823
115. Luo Y, Li J, Xu J, Zhu L, Han J, Zhang C (2018) Influence of pulsed arc on the metal droplet deposited by projected transfer mode in wire-arc additive manufacturing. J Mater Process Technol 259:353. https://doi.org/10.1016/j.jmatprotec.2018.04.047
116. Šmíd M, Kunz L, Hutař P, Hrbáček K (2014) High cycle fatigue of nickel-based superalloy MAR-M 247 at high temperatures. Proc Eng 74:329. https://doi.org/10.1016/j.proeng.2014.06.273
117. Sabol GP, Stickler R (1969) Microstructure of nickel-based superalloys. Phys Status Solidi 35:11. https://doi.org/10.1002/pssb.19690350102
118. Bhadeshia H (2000) Mechanically alloyed metals. Mater Sci Technol 16:1404–1411
119. Hosseini VA, Högström M, Hurtig K, Bermejo MAV, Stridh L-E, Karlsson L (2019) Wire-arc additive manufacturing of a duplex stainless steel: thermal cycle analysis and microstructure characterization. Weld World 63:975
120. Dharmendra C, Hadadzadeh A, Amirkhiz BS, Janaki Ram GD, Mohammadi M (2019) Microstructural evolution and mechanical behavior of nickel aluminum bronze Cu-9Al-4Fe-4Ni-1Mn fabricated through wire-arc additive manufacturing. Addit Manuf 30:100872. https://doi.org/10.1016/j.addma.2019.100872
121. Wang JF, Sun QJ, Wang H, Liu JP, Feng JC (2016) Effect of location on microstructure and mechanical properties of additive layer manufactured Inconel 625 using gas tungsten arc welding. Mater Sci Eng, A 676:395. https://doi.org/10.1016/j.msea.2016.09.015
122. Baufeld B (2012) Mechanical properties of INCONEL 718 parts manufactured by shaped metal deposition (SMD). J Mater Eng Perform 21:1416. https://doi.org/10.1007/s11665-011-0009-y
123. Shen C, Mu G, Hua X et al (2019) Influences of postproduction heat treatments on the material anisotropy of nickel–aluminum bronze fabricated using wire-arc additive manufacturing process. Int J Adv Manuf Technol 103:3199. https://doi.org/10.1007/s00170-019-03700-7
124. Ayan Y, Kahraman N (2022) Bending fatigue properties of structural steel fabricated through wire arc additive manufacturing (WAAM). Eng Sci Technol Int J 35:101247. https://doi.org/10.1016/j.jestch.2022.101247
125. Siddiqui SF, Araiza E (2023) Microstructural defects governing torsional fatigue failure of additively manufactured as-built and heat-treated Inconel 718. Eng Failure Anal 144:106975. https://doi.org/10.1016/j.engfailanal.2022.106975
126. Seow CE, Coules HE, Wu G, Khan RH, Xu X, Williams S (2019) Wire+ Arc Additively manufactured Inconel 718: effect of post-deposition heat treatments on microstructure and tensile properties. Mater Des 183:108157
127. Seow CE, Coules HE, Wu G, Khan RHU, Xu X, Williams S (2019) Wire + arc additively manufactured Inconel 718: effect of post-deposition heat treatments on microstructure and tensile properties. Mater Design 183:108157. https://doi.org/10.1016/j.matdes.2019.108157
128. Tanvir ANM, Ahsan MRU, Seo G et al (2020) Heat treatment effects on Inconel 625 components fabricated by wire + arc additively manufacturing (WAAM)—part 2: mechanical properties. Int J Adv Manuf Technol 110:1709. https://doi.org/10.1007/s00170-020-05980-w
129. Safarzade A, Sharifitabar M, Afarani MS (2020) Effects of heat treatment on microstructure and mechanical properties of Inconel 625 alloy fabricated by wire arc additive manufacturing process. Trans Nonferr Metals Soc China 30:3016
130. Dempster I, Cao W-D, Kennedy R, Bond B, Aurrecoechea J, Lipschutz M (2005) Structure and property comparison of Allvac® 718Plus™ alloy and Waspaloy forgings. In: Superalloys 718, 625, 706 and Derivatives. The Minerals, Metals & Materials Society (TMS), United States of America
131. Oguntuase O (2019) Development of post-deposition heat treatment to improve mechanical properties of wire-arc additive

manufactured ATI 718Plus superalloy. University of Manitoba, Canada. http://hdl.handle.net/1993/33902
132. Qiu Z, Wu B, Wang Z et al (2021) Effects of post heat treatment on the microstructure and mechanical properties of wire arc additively manufactured Hastelloy C276 alloy. Mater Charact 177:111158
133. Yin ZF, Zhao WZ, Lai WY, Zhao XH (2009) Electrochemical behaviour of Ni-base alloys exposed under oil/gas field environments. Corros Sci 51:1702. https://doi.org/10.1016/j.corsci.2009.04.019
134. Boissy C, Ter-Ovanessian B, Mary N, Normand B (2015) Correlation between predictive and descriptive models to characterize the passive film—study of pure chromium by electrochemical impedance spectroscopy. Electrochim Acta 174:430. https://doi.org/10.1016/j.electacta.2015.05.179
135. Mohammadi F, Nickchi T, Attar MM, Alfantazi A (2011) EIS study of potentiostatically formed passive film on 304 stainless steel. Electrochim Acta 56:8727. https://doi.org/10.1016/j.electacta.2011.07.072
136. Zhang Y, Chen Y, Li P, Male AT (2003) Weld deposition-based rapid prototyping: a preliminary study. J Mater Process Technol 135:347
137. Kong F, Ma J, Kovacevic R (2011) Numerical and experimental study of thermally induced residual stress in the hybrid laser–GMA welding process. J Mater Process Technol 211:1102
138. Wang J, Pan Z, Carpenter K, Han J, Wang Z, Li H (2021) Comparative study on crystallographic orientation, precipitation, phase transformation and mechanical response of Ni-rich NiTi alloy fabricated by WAAM at elevated substrate heating temperatures. Mater Sci Eng A 800:140307. https://doi.org/10.1016/j.msea.2020.140307
139. Lu X, Li MV, Yang H (2021) Comparison of wire-arc and powder-laser additive manufacturing for IN718 superalloy: unified consideration for selecting process parameters based on volumetric energy density. Int J Adv Manuf Technol 114:1517
140. Biswal R, Zhang X, Syed AK et al (2019) Criticality of porosity defects on the fatigue performance of wire+ arc additive manufactured titanium alloy. Int J Fatigue 122:208
141. Seow CE, Zhang J, Coules HE et al (2020) Effect of crack-like defects on the fracture behaviour of wire + arc additively manufactured nickel-base alloy 718. Addit Manuf 36:101578. https://doi.org/10.1016/j.addma.2020.101578
142. Artaza T, Bhujangrao T, Suárez A, Veiga F, Lamikiz A (2020) Influence of heat input on the formation of laves phases and hot cracking in plasma arc welding (PAW) additive manufacturing of Inconel 718. Metals 10:771
143. Ye X, Hua X, Wang M, Lou S (2015) Controlling hot cracking in Ni-based Inconel-718 superalloy cast sheets during tungsten inert gas welding. J Mater Process Technol 222:381
144. Dye D, Hunziker O, Reed R (2001) Numerical analysis of the weldability of superalloys. Acta Mater 49:683
145. Tammas-Williams S, Zhao H, Léonard F, Derguti F, Todd I, Prangnell PB (2015) XCT analysis of the influence of melt strategies on defect population in Ti–6Al–4V components manufactured by selective electron beam melting. Mater Charact 102:47
146. Xu X, Ding J, Ganguly S, Williams S (2019) Investigation of process factors affecting mechanical properties of INCONEL 718 superalloy in wire+ arc additive manufacture process. J Mater Process Technol 265:201
147. Lee J-Y, An J, Chua CK (2017) Fundamentals and applications of 3D printing for novel materials. Appl Mater Today 7:120. https://doi.org/10.1016/j.apmt.2017.02.004